

Dynamical dark energy models in the light of Gravitational-Wave Transient Catalogues

Celia Escamilla-Rivera^{1,*} and Antonio Nájera^{1,†}

¹*Instituto de Ciencias Nucleares, Universidad Nacional Autónoma de México,
Circuito Exterior C.U., A.P. 70-543, México D.F. 04510, México*

The study of current gravitational waves catalogues provide an interesting model independent way to understand further the *nature* of dark energy. Taking advantage of them, in this work we present an update of the constraints related to dynamical dark energy parameterisations using recent Gravitational-Wave Transient catalogues (GWTC1 and GWTC-2). Also, we present a new treatment for GW to establish the relation between the standard luminosity distance and the siren distance. According to our Bayesian results developed with our join SNeIa+CC+GW database, the Λ CDM model shows a preference against all the dark energy parameterisations considered here. Moreover, with the current GW transient database the GR standard luminosity and siren distances ratio shows a strong preference against the modified gravity δ -models considered here.

PACS numbers: 98.80.-k, 95.36.+x, 04.30.-w, 98.80.Es

1. INTRODUCTION

One of the current challenges of the precision cosmology is to understand the nature behind the late-cosmic acceleration. The study of a wide variety of observations, e.g. Cosmic Microwave Background Radiation (CMBR), Supernovas Type Ia (SNeIa), Baryonic Acoustic Oscillations (BAO) and the current Gravitational Waves (GWs) have been useful to constraint the cosmological parameters that define a specific cosmological model. Among these observations, some of them are consistent with the standard Λ CDM, which has its own theoretical and naturalness problems, so it is worthwhile to consider alternative options. A convenient road is to keep General Relativity (GR) as the gravitational theory and modify the stress-energy content of the universe –the so-called dark energy– i.e. we modify the right-hand side of the Einstein equations. A second road is to design an alternative theory of gravity, whose additional degrees of freedom can handle the cosmic acceleration –so-called the modified gravity method– via modifying the left-hand side of the Einstein equations, which leads to new physics on small cosmological scales. On the other hand, one of the most straightforward ways to explore a specific cosmic accelerated expansion is at a phenomenological level. In such a case, both roads can be quantified by the evolution of an equation of state (EoS) parameterisation (geometric in the case of modified gravity) of dark energy. Given the information on the values of the Hubble parameter H_0 , and the current matter density fraction, Ω_m , an arbitrary expression for the expansion evolution can be reproduced by assuming a flat Friedmann-Robertson-Walker (FRW) space-time with a dark energy component that has an EoS $w(z)$. Scenarios were a possible $w(z) \neq 1$ have been discussed extensively and this denotes a strong evidence of new gravitational physics and a possible new source of the cosmic acceleration. Fitting a constant w using observational data results in good agreement with a EoS value of -1 , but such analysis would have missed subtle variations in the EoS, as for example if the average happened to be near to -1 . Likewise, using a specific parametric form of $w(z)$ is liable to biasing the outcome. In this line of thought, some proposals have been currently studied, e.g. bidimensional dark energy models [1], EoS evolving with a scalar field dark energy [2], generic EoS derived from $f(R)$ [3–5], double exponential potentials for late-cosmic acceleration [6], interacting dark energy models like $w(q)$ [7], Padé approximants for dark energy [8] and dark energy inverse cosmography [9, 10].

Future proposals will be need to be addressed in the next decade by taking into account the discordance present between the different cosmological probes [11]. Recently, constraints derived from considering the interplay between GWs and other light gravitational degrees of freedom, related to dark energy, have been used to strongly restrict the latter. Also, with the help of the electromagnetic transient characteristic from the first multi-messenger observations of a binary neutron star merger [12], a possibility to constrain modified gravities emerged. In this matter, several classes of scalar-tensor theory were found incompatible with the GW data or else irrelevant to gravity at sufficiently large distances [13]. Some loopholes have been discussed by scanning a wider range of modified gravity theories such as Beyond Horndeski and DHOST [14].

The goal of this work is to present an update in the study of dark energy parameterisations by focusing on binary neutron stars with a counterpart detected through a gamma-ray burst (GRB), using Gravitational-Wave Transient Catalogues of Compact Binary Mergers observed by LIGO and Virgo during the first and second observing runs [15] in order to shed some light on their cosmological constraints.

*celia.escamilla@nucleares.unam.mx

†antonio.najera@correo.nucleares.unam.mx

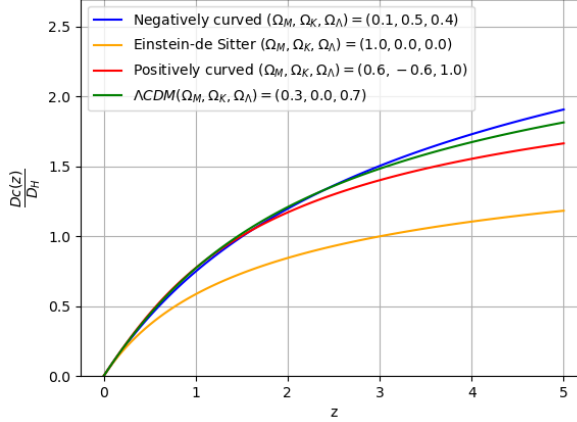


FIG. 1: Examples of the dimensionless comoving distance. We present four models: the Λ CDM model with $(\Omega_m, \Omega_K, \Omega_\Lambda) = (0.3, 0.0, 0.7)$, a positively curved model with $(\Omega_m, \Omega_K, \Omega_\Lambda) = (0.6, -0.6, 1.0)$, a negatively curved model with $(\Omega_m, \Omega_K, \Omega_\Lambda) = (0.1, 0.5, 0.4)$ and the Einstein-de Sitter model with $(\Omega_m, \Omega_K, \Omega_\Lambda) = (1.0, 0.0, 0.0)$.

This paper is organized as follows: In Sec.2 we will explain how distances in cosmology are written in standard way. This small introduction will encourage the search for the theoretical siren distance definition. In Sec.2.5 we will describe general properties to detect GWs and in Sec.3 their standard sirens. In Sec.4 we will present the theory behind the dark energy parameterisations. Some alternative bidimensional parametrisations are considered for the EoS, which deviate from the standard Λ CDM $w(z) = -1$. Among them, we will study the Chevallier-Polarski-Linder (CPL) [16] and the Low Correlation (LC) [17] parametrisations. In Sec.5 we will the observational compilations considered in this work. In Sec.6, we will perform the statistical analysis over the dark energy models discussed using the observational compilations including the GW catalogues. Finally, in Sec.7 we will discuss our main results.

2. COSMOLOGICAL DISTANCES

2.1. Comoving distance

Comoving distance D_C does not change with the expansion Hubble flow, therefore travelling in a small time dt as $dD_C = dD/a = cdt/a$ (since $c = dD/dt$) we can express

$$D_C(t) = c \int_t^{t_0} \frac{dt'}{a(t')}, \quad (1)$$

where t is the time of light emission and t_0 is the time of detection. This quantity can be also written as

$$D_C(z) = c \int_0^z \frac{dz'}{H(z')}, \quad (2)$$

with $H(z)$ as the Hubble parameter ($H(t) = (1/a)da/dt$). Defining $E(z) \equiv H(z)/H_0$, (2) can be written as

$$D_C(z) = D_H \int_0^z \frac{dz'}{E(z')}. \quad (3)$$

with D_H the Hubble distance ($D_H = c/H_0$). As an example, the dimensionless comoving distance (D_C/D_H) given for 4 different models is described in Figure 1.

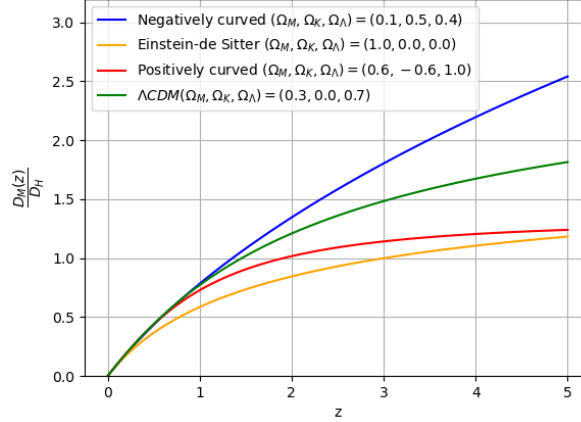


FIG. 2: Examples of the dimensionless transverse comoving distance. We present four models: the ΛCDM model with $(\Omega_m, \Omega_K, \Omega_\Lambda) = (0.3, 0.0, 0.7)$, a positively curved model with $(\Omega_m, \Omega_K, \Omega_\Lambda) = (0.6, -0.6, 1.0)$, a negatively curved model with $(\Omega_m, \Omega_K, \Omega_\Lambda) = (0.1, 0.5, 0.4)$ and the Einstein-de Sitter model with $(\Omega_m, \Omega_K, \Omega_\Lambda) = (1.0, 0.0, 0.0)$.

2.2. Transverse comoving distance

According to the Ω_K value, the transverse comoving distance (D_M) is defined as [18]:

$$D_M(z) = \begin{cases} \frac{D_H}{(\Omega_K)^{1/2}} \sinh \left[\frac{(\Omega_K)^{1/2} D_C(z)}{D_H} \right], & \text{for } \Omega_K > 0, \\ D_C(z), & \text{for } \Omega_K = 0, \\ \frac{D_H}{(-\Omega_K)^{1/2}} \sin \left[\frac{(-\Omega_K)^{1/2} D_C(z)}{D_H} \right], & \text{for } \Omega_K < 0. \end{cases} \quad (4)$$

The transverse comoving distance is defined as the ratio between the current transverse velocity with its proper motion [19]. Notice that if $\Omega_K = 0$, we obtain an expression equivalent to the comoving distance. In Figure 2 we discuss 4 possible cases for (4).

2.3. Angular diameter distance

The angular diameter distance is the ratio between the physical size of an object with its subtended angle, which in terms of the transverse comoving distance is denoted by [20]

$$D_A = \frac{D_M(z)}{1+z}. \quad (5)$$

At small z it is almost similar to the transverse comoving distance. The dimensionless angular diameter distance (D_A/D_H) for our four considered models is shown in Figure 3.

2.4. Luminosity distance

Another way to compute the distance to a source is to measure its flux F for an object of known luminosity L . The luminosity distance D_L is

$$D_L = \left(\frac{L}{4\pi F} \right)^{1/2}. \quad (6)$$

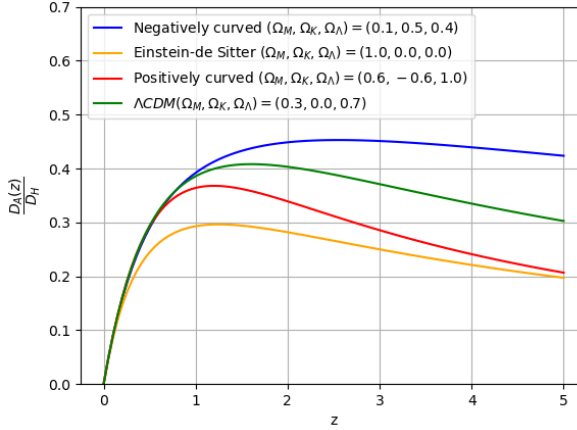


FIG. 3: Examples of the dimensionless angular diameter distance. We present four models: the Λ CDM model with $(\Omega_m, \Omega_K, \Omega_\Lambda) = (0.3, 0.0, 0.7)$, a positively curved model with $(\Omega_m, \Omega_K, \Omega_\Lambda) = (0.6, -0.6, 1.0)$, a negatively curved model with $(\Omega_m, \Omega_K, \Omega_\Lambda) = (0.1, 0.5, 0.4)$ and the Einstein-de Sitter model with $(\Omega_m, \Omega_K, \Omega_\Lambda) = (1.0, 0.0, 0.0)$.

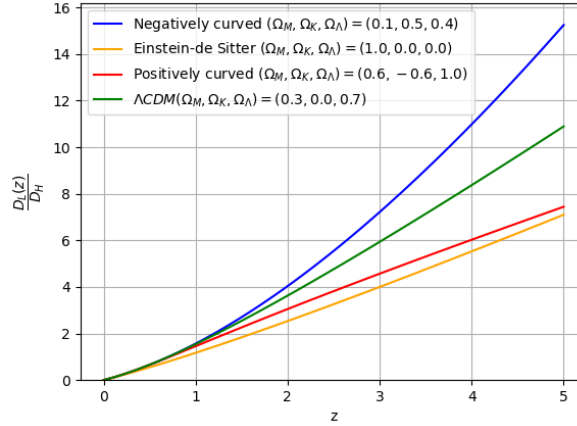


FIG. 4: Example of the dimensionless luminosity distance. We present four models: the Λ CDM model with $(\Omega_m, \Omega_K, \Omega_\Lambda) = (0.3, 0.0, 0.7)$, a positively curved model with $(\Omega_m, \Omega_K, \Omega_\Lambda) = (0.6, -0.6, 1.0)$, a negatively curved model with $(\Omega_m, \Omega_K, \Omega_\Lambda) = (0.1, 0.5, 0.4)$ and the Einstein-de Sitter model with $(\Omega_m, \Omega_K, \Omega_\Lambda) = (1.0, 0.0, 0.0)$.

The luminosity distance can be written in terms of the angular diameter distance and the transverse comoving distance as [20]

$$D_L(z) = (1 + z)D_M = (1 + z)^2 D_A. \quad (7)$$

The dimensionless luminosity distance (D_L/D_H) for the four considered models is shown in Figure 4.

2.5. Standard sirens distance

In GR, GWs have two transverse polarizations [21]. Each polarization are denoted by h_+ and h_\times .

Let us design a ring of free particles where a GW arrive. By considering two well-chosen test masses (see Figures 5 and 6) we can calculate their distance to the center to see if a GW is causing a perturbation. In the first half cycle, the distance to the center of one test mass will increase, while the other will decrease. In the second half cycle, it is on reverse. By building an interferometer a passing space-time perturbation would produce a time-varying distance that can be analysed to detect the GW. Unfortunately, the changes in distances by astrophysical situations are minimal because of the tiny amplitudes [22]. This is the reason of why a very sensitive interferometer is required in the experiment.

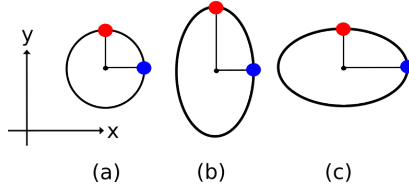


FIG. 5: (a) A ring of particles initially at rest. (b) The ring of particles distorted by a h_+ at $\pi/4$ phase. (c) The distortion at phase $3\pi/2$. Two test masses are being considered.

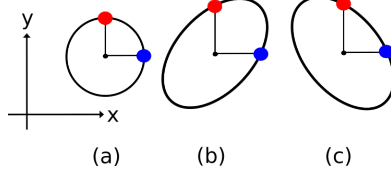


FIG. 6: (a) A ring of particles initially at rest. (b) The ring of particles distorted by a h_x at $\pi/4$ phase. (c) The distortion at phase $3\pi/2$. Two test masses are being considered.

If a GW with h_+ that is traveling in the z -direction hits a circular ring initially at rest (the phase of the GW when it hits the ring is assumed 0) in the $x - y$ plane the particles will be moved in the way shown in Figure 5. Since the GW is periodic, (b) and (c) will be repeated every half cycle. The case for a h_x wave is shown in Figure 6. An arbitrary GW will be a linear combination of these two polarization states.

The tensor h_{ij} of a GW can be expressed (this derivation is performed in Appendix A) as

$$h_{ij} = \frac{2G}{c^4 D_S} \left[\frac{d^2 I_{ij} \left(t - \frac{R}{c} \right)}{dt^2} \right]^{TT}, \quad (8)$$

where I_{ij} denotes the quadrupole moment tensor and TT is the transverse and traceless part of I_{ij} . By integrating the instantaneous energy flux gravitational radiation over all directions the luminosity of a GW can be computed as [23]

$$\mathcal{L} = \frac{G}{5c^2} \left[\frac{d^3 I_{ij}^{TT}}{dt^3} \frac{d^3 I^{ij \, TT}}{dt^3} \right]. \quad (9)$$

Hence the time average over a period can be written as

$$\mathcal{L} = \frac{G}{5c^2} \left\langle \frac{d^3 I_{ij}^{TT}}{dt^3} \frac{d^3 I^{ij \, TT}}{dt^3} \right\rangle. \quad (10)$$

The transverse and traceless part was taken into account, which means that it is being considered the non-spherical motion of the GW source, hence only the kinetic energy in the non-spherical motion contributes to the emission of energy of a GW.

We can derive the amplitude of the system considering an inspiralling binary system with M as the total mass. Also, it is convenient to consider their reduced mass $\mu = m_1 m_2 / M$, since the kinetic energy of the system is $K = \mu v^2 / 2$. Using Kepler's third law we can compute the amplitude of a GW

$$\frac{T^2}{r^3} = \frac{4\pi^2}{GM}, \quad (11)$$

where T and r denotes the period of the orbit and the distance between the masses, respectively. We can rewrite the latter equation in terms of the velocity of rotation if $v = 2\pi r/T$ and $v^2 = GM/r$. By inserting the kinetic energy of the system into (8) the amplitude of a GW is [22]

$$h \approx \frac{G^2 \mu M}{D_S r c^4}, \quad (12)$$

where D_S is the siren distance to the source and r the distance between the binaries. As an example, we can consider a couple of $10M_\odot$ mass binaries, so that the total mass is $20M_\odot$ at a siren distance of 200 Mpc and separated by $r = GM_\odot/c^2$, therefore the amplitude is $h \approx 2.39 \times 10^{-20}$.

3. DYNAMICS

Using (10), the luminosity of a GW created by an inspiralling binary is [23]

$$\mathcal{L} = \frac{32\mu^2 G^4 M^3}{5r^5 c^5}. \quad (13)$$

This is the observational luminosity, from which the observational luminosity siren distance can be computed by deriving the dynamics of the system. Since binaries emit energy in the form of GWs, their kinetic energy must be reduced and therefore the orbit radius decreases with time, and eventually the binaries collide with each other. To compute this rate of change of the orbit radius we can consider the following ansatz: if the entire bond energy of the system (which is $E = \mu v^2/2$) transforms into luminosity energy, then

$$\mathcal{L} = -\frac{dE}{dt}. \quad (14)$$

Using Kepler's third law to write the bond energy in function of the radius $E = \mu GM/2r$, where M is the total mass of the system, therefore

$$\mathcal{L} = -\frac{\mu GM}{r^2} \frac{dr}{dt}. \quad (15)$$

Solving for dr/dt we obtain

$$\frac{dr}{dt} = -\frac{64G^3\mu M^2}{5r^3 c^5}, \quad (16)$$

which can be rewritten in terms of the angular frequency of rotation and $T = 2\pi/\omega$, the distance between the binaries is given by

$$r = \left(\frac{GM}{\omega^2} \right)^{1/3}, \quad (17)$$

and (16) in terms of the angular frequency is

$$\frac{d\omega}{dt} = \frac{96\mu}{5c^5} (\omega^{11} G^5 M^2)^{1/3}. \quad (18)$$

The orbital and GW frequency of the binaries are related by $f_{\text{GW}} = f_{\text{orbital}}/2 = \omega/\pi$, then

$$\frac{df_{\text{GW}}}{dt} = \frac{96\mu\pi^{8/3}}{5c^5} (f_{\text{GW}}^{11} G^5 M^2)^{1/3}. \quad (19)$$

Combining (12) and (19) we can obtain the siren distance for a GW

$$D_S = \frac{5c}{96\pi^2 h f_{\text{GW}}^3} \frac{df_{\text{GW}}}{dt}. \quad (20)$$

This expression allows us to measure the siren luminosity distance, the frequency and the strain as a function of time¹. The amplitude h and the strain are related by solving the geodesic deviation equation, then $h \approx \Delta L/L$ (where L is the distance between some test masses and ΔL is the strain). Therefore, Eq.(20) can be computed with the observables of a GW. The time it

¹ From this we can determine the quantity df_{GW}/dt [24].

takes to the binaries to coalesce can also be computed by integrating (19). The lifetime of the system (so called the *chirp* time (t_c)) from an initial radius r_0 at an initial frequency f_0 GW is given by

$$t_c = \frac{5c^5}{256\mu} \left(\frac{1}{\pi^8 f_0^8 G^5 M^2} \right)^{1/3}. \quad (21)$$

In comparison to the other definitions of distances described, a theoretical siren luminosity distance is required at this point. The experimental distance was derived in (20) and experiments that detect GWs report them along with the redshift of the event, so that the theoretical is the quantity to determine. A possible form is proposed in [25] where a relationship between the standard luminosity and the siren luminosity distance is given by

$$D_S(z) = D_L(z) \exp \left(- \int_0^z \frac{\delta(z')}{1+z'} dz' \right), \quad (22)$$

which comes from a modified gravity model. The subscript S and L denotes the siren luminosity distance and the standard candle luminosity distance, respectively. To analyse data coming from GWs, the form of $\delta(z)$ needs to be found.

In this work we consider three forms of delta functions from [26]. These deltas are defined as:

$$\delta_1(z) = \frac{n(1-\Xi_0)}{1-\Xi_0 + \Xi_0(1+z)^n}, \quad (23)$$

$$\delta_2(z) = \frac{n(1-\Xi_0)(1+z)^{n-1}}{1+\Xi_0(\exp(z^n)-1)}, \quad (24)$$

$$\delta_3(z) = \frac{n(1-\Xi_0)}{1-\Xi_0 + \Xi_0(1+z)^n} + \frac{n(1-\Xi_0)}{(1+z)^n} - \frac{2n(1-\Xi_0)}{(1+z)^{2n}}, \quad (25)$$

where the quantities n and Ξ_0 are both positive and given by [25]

$$\begin{aligned} \Xi_0 &= \lim_{z \rightarrow \infty} \frac{M^*(0)}{M^*(z)}, \\ n &\approx \frac{\alpha_{M0}}{2(\Xi_0 - 1)}. \end{aligned} \quad (26)$$

The GR case can be recover when $\Xi_0 = 1$ [26] and its delta is

$$\delta_{\text{GR}}(z) = 0. \quad (27)$$

By inserting (23), (24), and (25) into (22) and integrating, the siren distances are

$$D_{S_1}(z) = D_L(z) \left(\Xi_0 + \frac{1-\Xi_0}{1+z^n} \right), \quad (28)$$

$$D_{S_2}(z) = D_L(z) [\Xi_0 + (1-\Xi_0) \exp(-z^n)], \quad (29)$$

$$D_{S_3}(z) = D_L(z) \exp \left(- \frac{(1-\Xi_0)(1-(1+z)^n)}{(1+z)^{2n}} \right) \times \left(\Xi_0 + \frac{1-\Xi_0}{1+z^n} \right), \quad (30)$$

Finally, the GR case can be achieved by the ratio

$$D_{S_{\text{GR}}}(z) = D_L(z). \quad (31)$$

It is useful to analyse the limits of (28), (29), and (30): when $z \rightarrow 0$, $D_S(z) = D_L(z)$, and when $z \rightarrow \infty$, $D_S(z) \rightarrow D_L(z)\Xi_0$. Therefore, at $z = 0$, both distances are equal and at early times their ratio goes to a positive constant. Also, if $\Xi_0 = 1$, $D_S(z) = D_L(z)$, the ratio with these distances holds for every z . In this work we also develop these parameterisations over δ to study the consequences in the dark energy dynamics.

4. DYNAMICAL DARK ENERGY PARAMETERISATIONS

Since the concordance cosmological Λ CDM model has several theoretical problems [27], new proposals have been presented along these years. One of the most popular is related to the addition of an exotic fluid denoted as dark energy. Furthermore, modifications of the gravity itself [28] also have been considered.

Several dark energy EoS w have been built to describe the late cosmic acceleration. To see which one of them has more constraining power we test them using observational data.

The fact that the universe is experimenting an accelerated expansion direct us to consider a negative pressure component at late times. Since the energy is always positive, the dark energy EoS $w = w(z)$ requires to be ($w(z) = P/\rho < -1/3$). For a spatially flat universe

$$E(z) = \left(\frac{H(z)}{H_0} \right) = [\Omega_m(1+z)^3 + \Omega_\Lambda f(z)]^{1/2}, \quad (32)$$

where the function $f(z)$ is defined as

$$f(z) = \exp \left(3 \int_0^z \frac{1+w(z')}{1+z'} dz' \right), \quad (33)$$

for a given $w(z)$ the dynamics of the expansion is determined. The Λ CDM model is a special case when $w(z) = -1$, $f(z) = 1$. From here, we can consider the following six bidimensional² dark energy parameterisations³ with different analytical forms of $w(z)$.

4.1. Lambda Cold Dark Matter-redshift (Λ CDM)

This cosmological model is represented by $w(z) = -1$, so the Friedmann equation becomes

$$E(z)^2 = \Omega_m(1+z)^3 + (1-\Omega_m). \quad (34)$$

This is a simple model that describes the late-time cosmic acceleration.

4.2. Chevallier-Polarski-Linder (CPL)

Another parameterization considers an EoS [16, 29] of the form

$$w(z) = w_0 + \left(\frac{z}{1+z} \right) w_1, \quad (35)$$

which converges for high redshift and also reduces to the Λ CDM model for $w_1 = 0$ and $w_0 = -1$. In this case the Friedmann equation is

$$\begin{aligned} E(z)^2 = & \Omega_m(1+z)^3 + (1-\Omega_m) \exp \left(-\frac{3w_1 z}{1+z} \right) \\ & \times (1+z)^{3(1+w_0+w_1)}. \end{aligned} \quad (36)$$

4.3. Barboza-Alcaniz (BA)

This model proposes an EoS [30] of the form

$$w(z) = w_0 + \frac{z(1+z)}{1+z^2} w_1. \quad (37)$$

² We denoted *bidimensional* as the dependence solely of two free theoretical parameters w_i

³ A previous analysis of these models have been presented in [1]

Notice that this expression does not diverge for $z \rightarrow -1$. In this case the Friedmann equation is

$$E(z)^2 = \Omega_m(1+z)^3 + (1-\Omega_m)(1+z)^{3(1+w_0)} \times (1+z^2)^{3w_1/2}. \quad (38)$$

4.4. Jassal-Bagla-Padmanabhan (JBP)

This parameterization has an EoS given by [31]

$$w(z) = w_0 + \frac{z}{(1+z)^2} w_1, \quad (39)$$

which converges for high redshifts and contains a dark energy contribution at this scale. The Friedmann equation for this parameterization is

$$E(z)^2 = \Omega_M(1+z)^3 + (1-\Omega_M) \times \exp\left(\frac{3w_1 z^2}{2(1+z)^2}\right) (1+z)^{3(1+w_0)}. \quad (40)$$

4.5. Linear-redshift (LR)

The EoS for this model is given by $w(z) = w_0 - w_1 z$ [32] and it can be reduced to Λ CDM when $w_0 = -1$ and $w_1 = 0$. With this EoS the $f(z)$ can be computed and the Friedmann equation becomes

$$E(z)^2 = \Omega_m(1+z)^3 + (1-\Omega_m) \exp(-3w_1 z) (1+z)^{3(1+w_0+w_1)}. \quad (41)$$

For high redshift this EoS diverges. This gives strong constraints on the value of w_1 .

4.6. Low Correlation (LC)

This is a model with an EoS [17] given by

$$w(z) = \frac{(-z+z_c)w_0 + z(1+z_c)w_c}{(1+z)z_c}, \quad (42)$$

where $w_0 = w(0)$ and $w_c = w(z_c)$ and z_c is a given redshift value so that (w_0, w_c) are uncorrelated. These values depend on the data used to be constrained. This parameterization reduces to Λ CDM for $w_0 = -1$ and $w_c = -1$. The Friedmann equation is

$$E(z)^2 = \Omega_m(1+z)^3 + (1-\Omega_m) \times \exp\left(\frac{9(w_0-w_c)z}{1+z}\right) (1+z)^{3(1-2w_0+3w_c)}. \quad (43)$$

4.7. Wetterich-redshift (WP)

This parameterization is given by [33]

$$w(z) = \frac{w_0}{(1+w_1 \ln(1+z))^2}, \quad (44)$$

where the Friedmann equation is

$$E(z)^2 = \Omega_m(1+z)^3 + (1-\Omega_m) \times (1+z)^{3\left(1+\frac{w_0}{1+w_1 \ln(1+z)}\right)}. \quad (45)$$

5. OBSERVATIONAL COMPILATIONS

It is well known that the dark energy domination era began at a late period in the evolution of the universe. Then the best data to study this dark component is at low redshifts. In this section we explain the method to obtain the cosmological parameters Ω_m , $\Theta = \{w_0, w_1\}$, $h = H_0/(100 \text{ km s}^{-1} \text{ Mpc}^{-1})$. We perform these analyses using the Λ CDM model and the six bidimensional models described. We start by using the SNeIa and Cosmic Chronometers compilations, once this is done, we will implement the GW catalogues data to improve the constraints over the cosmological parameters.

5.1. Pantheon supernovae compilation

The Pantheon catalogue [34] includes $N_{\text{Pantheon}} = 1048$ events. These events are treated in an interval $z \in [0.010, 2.26]$. To compute the statistical analysis of this sample we use

$$\mu(z_i, \mu_0) = 5 \log_{10} \left(\frac{D_L(z)}{10 \text{ pc}} \right), \quad (46)$$

where $D_L(z)$ is given by (7). The best fit parameters Ω_m , $\Theta = \{w_0, w_1\}$, h can be calculated by maximizing the logarithm of the likelihood function [35]

$$\ln p(\mu(z)|z, \sigma, h, \Omega_m, \Theta) = -\frac{1}{2} \left(\chi^2 + \sum_{n=1}^{N_{\text{Pantheon}}} \ln(2\pi\sigma_{\text{obs}}^2) \right), \quad (47)$$

where the χ^2 is given by

$$\chi^2 = \sum_{n=1}^{N_{\text{Pantheon}}} \frac{(\mu(z_n, \Omega_m, \Theta) - \mu_{\text{obs}}(z_n))^2}{\sigma_{\text{obs}}^2}, \quad (48)$$

with $\sigma_{n \text{ obs}}^2$ the measurement variances.

5.2. Cosmic Chronometers compilation

This database includes $N_{\text{CC}} = 52$ events in the redshift interval $z \in [0, 2.36]$ [36]. In comparison to SNeIa data, the logarithm of the likelihood function (47) is expressed as the difference between the function $H(z)$ instead of $\mu(z)$. The χ^2 function for this case given by

$$\chi^2 = \sum_{i=1}^{N_{\text{Hubble}}} \frac{(H(z_i, \Omega_M, w_0, w_1) - H_{\text{obs}}(z_i))^2}{\sigma_{n \text{ obs}}^2}, \quad (49)$$

where and H_{obs} and $\sigma_{n \text{ obs}}$ correspond to the observations and their errors, respectively.

5.3. Gravitational-Wave Transient Catalogue GWTC-1

This catalogue includes $N_{\text{GWTC-1}} = 11$ confident detection events in redshift range of $z \in [0.01, 0.49]$ from gravitational-wave searches for coalescing compact binaries, all of them with masses $M > 1M_{\odot}$. These events observed by LIGO⁴ and Virgo⁵ come from the first and second observing runs [37]. In Table III from [37], the 11 events are reported along with their observational siren distances D_S in Mpc and redshifts z and other several observational variables, all of them with their corresponding 90% credible variances.

With the latter information, the natural logarithm of the likelihood function for the GWTC-1 catalogues can be compute using the following expression

⁴ <https://www.ligo.caltech.edu>

⁵ <http://www.virgo.infn.it>

$$\ln p(D_S \text{GWTC-1} | z, \sigma, h, \Omega_m, w_0, w_1, n, \Xi_0) = -\frac{1}{2} \left(\chi^2 + \sum_{j=1}^{N_{\text{GWTC-1}}} \ln(2\pi\sigma_j^2 \text{obs, GWTC-1}) \right), \quad (50)$$

where

$$\chi_{\text{GWTC-1}}^2 = \sum_{j=1}^{N_{\text{GWTC-1}}} \frac{(D_S(z_j, h, \Omega_m, w_0, w_1, n, \Xi_0) - D_S \text{obs, GWTC-1}(z_j))^2}{\sigma_j^2 \text{obs, GWTC-1}}. \quad (51)$$

The GWTC-1 catalogue includes variances in z , therefore the squared variances are

$$\sigma_j^2 \text{obs, GWTC-1} = \sigma_j^2 D_S \text{obs, GWTC-1} + \sigma_j^2 z \text{obs, GWTC-1}. \quad (52)$$

Notice that the squared variances of the siren distance per redshift are added. But since the upper and lower reported variances are not equal, the biggest of each case were taken as the variance. Then the logarithm of the likelihood function is maximized and we run Markov Chains in order to get the best fit values of $h, \Omega_m, w_0, w_1, \Xi_0$, and n and their confidence regions.

5.4. Gravitational-Wave Transient Catalogue GWTC-2

This second GW catalogue includes $N_{\text{GWTC-2}} = 39$ candidate GW events, with less than 10% of contamination fraction in the redshift range $z \in [0.03, 0.8]$ from the first half of the third observable run [38]. In Table VI from [38] these events measured by LIGO-Virgo are presented with their observational siren distances D_S in Gpc⁶ and redshifts z , along with other several observational variables, all of them with their corresponding 90% credible variances.

The logarithm of the likelihood function for the GWTC-2 catalogue is given by

$$\ln p(D_S \text{GWTC-2} | z, \sigma, h, \Omega_m, w_0, w_1, n, \Xi_0) = -\frac{1}{2} \left(\chi^2 + \sum_{j=1}^{N_{\text{GWTC-2}}} \ln(2\pi\sigma_j^2 \text{obs, GWTC-2}) \right), \quad (53)$$

where

$$\chi_{\text{GWTC-2}}^2 = \sum_{j=1}^{N_{\text{GWTC-2}}} \frac{(D_S(z_j, h, \Omega_m, w_0, w_1, n, \Xi_0) - D_S \text{obs, GWTC-2}(z_j))^2}{\sigma_j^2 \text{obs, GWTC-2}}. \quad (54)$$

The GWTC-2 catalogue includes variances in z described by

$$\sigma_j^2 \text{obs, GWTC-2} = \sigma_j^2 D_S \text{obs, GWTC-2} + \sigma_j^2 z \text{obs, GWTC-2} \quad (55)$$

Both squared variances of the siren distance and redshift are considered. And as in the GWTC-1 database the upper and lower reported variances are not equal, then the biggest of each case was taken as the variance. Then logarithm of the likelihood function is maximized and we run again Markov Chains in order to get the best fit values of $h, \Omega_m, w_0, w_1, \Xi_0$, and n and their confidence regions. The analysis is done with the sum of the GWTC-1 and GWTC-2 databases, we denote the join likelihood as ‘GW database’. Due that this database reports events with less than 10% of contamination fraction, the best fit values and their confidence regions will be biased a little. Moreover, this bias will be minimal due the density of data when combining it with Pantheon and CC data, so that the GWTC-2 that contains the bias represents just the 3.39% of the total Pantheon+CC+GW database.

6. METHODOLOGY

Once the best cosmological parameters were obtained by maximizing the logarithm of the likelihood function, the Monte Carlo Markov chains to get the σ and 2σ confidence regions were obtained using a modified version of emcee [39]. The confidence regions plots and best fit values with their $1-\sigma$ uncertainties were made by using the GetDist software ([40] and references therein).

⁶ Our units conversion must be performed to be consistent with the GWTC-1 database, where the D_S is reported in Mpc.

Information Criteria	Preference for model \mathcal{M}_i
$0 < \Delta\text{BIC}, \Delta\text{AIC} < 2$	Weak
$2 \leq \Delta\text{BIC}, \Delta\text{AIC} < 6$	Definite
$6 \leq \Delta\text{BIC}, \Delta\text{AIC} < 10$	Strong
$10 \leq \Delta\text{BIC}, \Delta\text{AIC} < 12$	Very strong

TABLE I: Revised Jeffreys scale used to interpret the values of $\ln B$ obtained when comparing two competing models through their Bayesian evidence. A value of $\ln B > 0$ indicates that the extended model is favoured with respect to the ΛCDM baseline model.

6.1. Statistical analysis

The best fit values and the $1-\sigma$ uncertainties for the h, Ω_m, w_0 , and w_1 parameters using Pantheon and CC databases and their overlapping are reported in Table II. The best fit values and the $1-\sigma$ uncertainties for the $h, \Omega_m, w_0, w_1, \Xi_0, n$ parameters for the case of the GW database along with their overlapping with Pantheon and CC are reported in Tables III, IV and V, one for each siren delta function δ_1, δ_2 and δ_3 , respectively.

We also include in the analysis the plots at $1-\sigma$ and $2-\sigma$ confidence regions for the seven models (including ΛCDM model with the six bidimensional dark energy parameterisations). These analyses include for each model:

1. Analysis performed using Pantheon compilation, CC data, and their overlap Pantheon+CC. See Figures 7-9-11-13-15-17-19.
2. Analysis performed per siren delta function using Pantheon compilation, the overlap Pantheon+CC and GW data. See Figures 8-10-12-14-16-18-20.
3. Analysis performed per siren delta function using GW data, the overlap Pantheon+GW, and the overlap Pantheon+CC+GW. See Figure 21.

6.2. Information Criteria analysis

We performed a Markov-chain Monte Carlo (MCMC) analysis using a modified version of the emcee code⁷ interfaced to the publicly available sampling code MontePython-v3⁸ [41, 42]. We obtained plots using the GetDist package⁹ [40]. We sampled over the parameters $\{h_0, \Omega_m, \Theta, \Xi_0, n\}$ using the Metropolis-Hastings method and with a Gelman-Rubin [43] convergence criteria around $R - 1 < 0.03$. To quantify to what extent the improvement in our fit to the database described warrants the increase in the model complexity compared to the ΛCDM model, we compute the Bayes factor –the ratio of the evidences for the extended model \mathcal{M}_E with respect to the baseline \mathcal{M}_L – as [44]:

$$B_{EL} \equiv \frac{\int d\boldsymbol{\theta}_E \pi(\boldsymbol{\theta}_E | \mathcal{M}_E) \mathcal{L}(\mathbf{x} | \boldsymbol{\theta}_E, \mathcal{M}_E)}{\int d\boldsymbol{\theta}_L \pi(\boldsymbol{\theta}_L | \mathcal{M}_L) \mathcal{L}(\mathbf{x} | \boldsymbol{\theta}_L, \mathcal{M}_L)}, \quad (56)$$

where $\pi(\boldsymbol{\theta}_{E, L})$ is the prior for the parameters $\boldsymbol{\theta}_{E, L}$ and $\mathcal{L}(\mathbf{x} | \boldsymbol{\theta}_{E, L})$ the likelihood of the data given the model $\mathcal{M}_{E, L}$. The extent to what the extended model \mathcal{M}_E is preferred over the baseline \mathcal{M}_L can be qualitatively assessed using the Jeffreys scale reported in Table I. We compute the evidence directly from our MCMC using the method introduced in Ref. [45] implemented in the MCEvidence code¹⁰.

We compared the six dark energy parameterisations against the ΛCDM model with the Pantheon+CC+GW dataset using the Akaike Information Criteria (AIC) and the Bayesian Information Criteria (BIC) [46, 47]. The AIC is given by [46]

$$\text{AIC} = \chi^2_{\text{Pantheon+CC+GW min}} + 2k, \quad (57)$$

where $\chi^2_{\text{Pantheon+CC+GW min}}$ is the minimum χ^2 given by the sum of χ^2 s of the Pantheon+CC+GW data, and k the number of parameters of the model. Meanwhile, the BIC is given by [46]

$$\text{BIC} = \chi^2_{\text{Pantheon+CC+GW min}} + k \ln N, \quad (58)$$

⁷ <https://emcee.readthedocs.io>

⁸ https://github.com/brinckmann/montepython_public

⁹ <https://getdist.readthedocs.io/en/latest>

¹⁰ <https://github.com/yabebalFantaye/MCEvidence>

where N is the number of elements of the dataset, for Pantheon+CC+GW it is $N = 1150$. When comparing models, the one with smaller AIC and BIC is preferred and the strength of the preference is given by the Jeffrey's criterion (see Table I) [26, 47] with $\Delta\text{AIC} = |\text{AIC}_{\text{model 1}} - \text{AIC}_{\text{model 2}}|$ and $\Delta\text{BIC} = |\text{BIC}_{\text{model 1}} - \text{BIC}_{\text{model 2}}|$. We present the results of these analyses in Tables VI, VII and VIII.

To see whether one of the three siren delta functions (23), (24), (25) or the ratio between the siren distance and luminosity distance ($D_S(z) = D_L(z)$) derived from GR is better, we performed the AIC and BIC analyses by comparing the three deltas against GR. For this analysis we considered the constraints obtained from the six dark energy models along with the ΛCDM model using the full GW database. We present these results in Table IX.

As it can be seen in the plots, the ΛCDM model ($w_0 = -1$) and the LC model ($w_1 = 0, w_c = -1$) lies within the 2σ uncertainties for all the cases and databases. Also, for all the cases and databases containing GW data, the equivalence of the siren distance D_S with the luminosity distance D_L ($D_S = D_L$) lies within the 1σ uncertainty. Therefore, this ratio is consistent with the current GW data, and also it is the best model.

According to the values reported in Table III, current GW transient data is not able to constrain the value of Ω_m , w_1 and n . When an overlap of GW with other database was done the values of Ω_m , w_1 were almost GW-non-dependent. Also, since the definitions for Pantheon and CC data do not contain the n parameter, a best fit value for this parameter cannot be computed, because the form of the graphic of n in all cases was non-gaussian like. However, GW data was able to constrain the value of Ξ_0 , which is consistent with the ratio $D_S = D_L$, and gives a clue that both distances are equivalent. Future GW databases will decide either this ratio holds or not, and also might constrain the n value.

As we can see in Tables VI, VII, and VIII, since ΛCDM has the smallest AIC and BIC in all cases (for the three deltas and the six dark energy models), it is the best model with the current Pantheon+CC+GW data. How preferred is the ΛCDM model over the six dark energy parameterisations was computed with the Jeffrey's criterion. For the AIC criterion the preference is very weak, but with the BIC criterion ΛCDM has a very strong preference against the other models. Hence, the best model by far with our dataset is ΛCDM . But, among the dark energy parameterisations, BA was the preferred model because it has the lower AIC and BIC values, for the three deltas.

In the case of the deltas against GR, their values are reported in Table IX, GR is the best model ($D_L(z) = D_S(z)$) since it has in all the models the smallest AIC and BIC. The GW database is small ($N_{\text{GW}} = 50$) and the GTC-2 catalogues that forms part of this database include a contamination of less than 10%, so that a bias of less than 10% must be present in the analysis. Therefore, the results should not be extremely accurate, but with AIC, GR has a positive preference over δ_1 , δ_2 , and δ_3 . Meanwhile, according to the BIC, GR has a strong preference over the same deltas. Therefore the GR case is the best with the current GW database. Furthermore, the luminosity distance (D_L) and the siren distance (D_S) ratio is better than the expressions (28), (29), and (30) with the current GW database. Among the three deltas, δ_3 was the best by a minimum difference because it has the lowest AIC and BIC, except for the CPL case in which δ_2 is the best parameterisation.

Furthermore, we computed the ratio between the siren distance and the luminosity distance for the case δ_3 using the AIC and BIC criteria for the ΛCDM model, the six dark energy parameterisations, and the GR case. This ratio is shown in Figure 22 using the delta functions for these models.

7. CONCLUSIONS

Our first task in this work was to present an update analysis of the six dark energy parameterisations using the new GW databases described. We consider current SNeIa (Pantheon)+CC+GW data, the GW data came from the GWTC-1 [37] and GWTC-2 [38] catalogues. With this new database, the ΛCDM had a preference against the six dark energy considered models according to the BIC.

The second task was to study the siren distance of GWs. This was performed using the siren delta functions that give three different siren distance - luminosity distance relationships. They were compared against the GR ratio case, which had a positive preference with the AIC and strong preference with the BIC. As a result, the ratio between the siren distance and the luminosity distance is the best model.

Although the standard models (ΛCDM and GR) were preferred against the bidimensional dark energy parameterisations and the ratio between siren distance-luminosity distance, GWs have opened the door to update the previous analysis with supernovae and CC data with GW data. Future GW data might give more clues to discover the actual nature of dark energy, whether it is ΛCDM or another one. The analyses done in this work can be improved with future more numerous and accurate data. Even though the ΛCDM model was preferred, future higher redshift in GW data (due that GWTC-1 and GWTC-2 do not exceed $z = 1$) might change the preferences of GR over the siren distance-luminosity distance coming from modified gravity models. This study will be reported elsewhere.

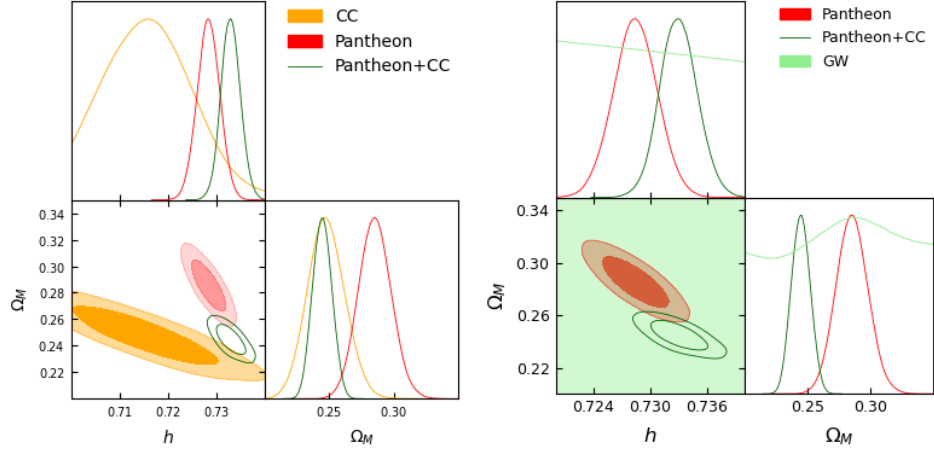


FIG. 7: 1- σ and 2- σ confidence contours for the cosmological parameters h and Ω_M for the Λ CDM model. *Left*: Analyses performed using Pantheon compilation (red color) and CC data (orange color). *Right*: Analyses performed using Pantheon compilation, CC data and GW catalogues (green color).

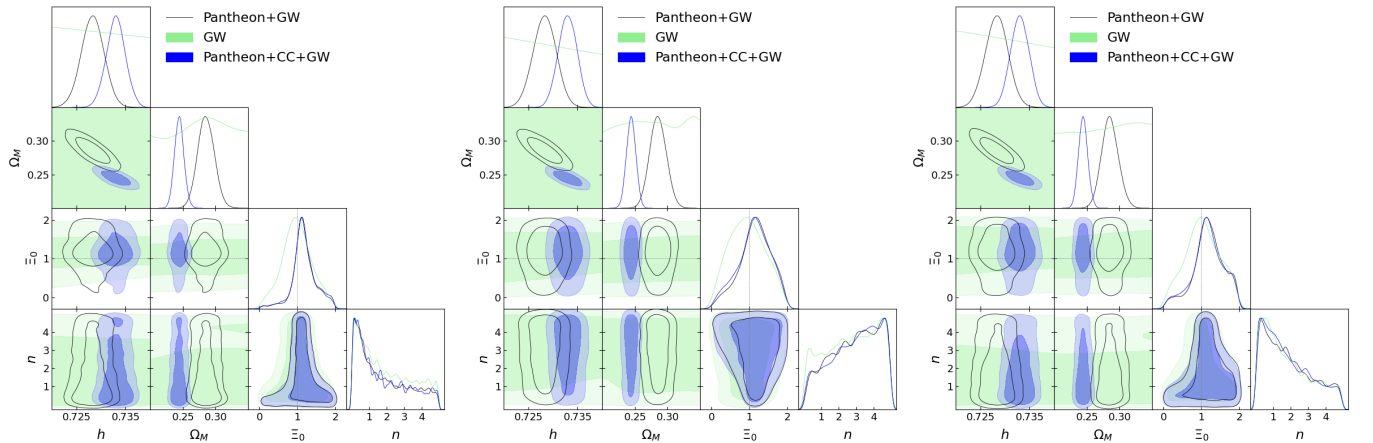


FIG. 8: 1- σ and 2- σ confidence contours for the cosmological parameters in Λ CDM h , Ω_M , Ξ_0 and n using the combinations of samples: Pantheon+GW (black color), GW catalogues (green color) and Pantheon+CC+GW (blue color). *Left*: case with δ_1 , *middle*: case with δ_2 and *right*: case with δ_3 .

Acknowledgments

CE-R acknowledges the *Royal Astronomical Society* as FRAS 10147. CE-R and AN are supported by PAPIIT Project IA100220. This article is also based upon work from COST action CA18108, supported by COST (European Cooperation in Science and Technology). Numerical computations for this research were done in the Tochtili ICN-UNAM cluster.

[1] Celia Escamilla-Rivera. Status on bidimensional dark energy parameterizations using SNe Ia JLA and BAO datasets. *Galaxies*, 4(3):8, 2016.

[2] Celia Escamilla-Rivera, Luciano Casarini, Julio C. Fabris, and Jailson S. Alcaniz. Linear and non-linear perturbations in dark energy models. *JCAP*, 11:010, 2016.

[3] Luisa G. Jaime, Mariana Jaber, and Celia Escamilla-Rivera. New parametrized equation of state for dark energy surveys. *Phys. Rev. D*, 98(8):083530, 2018.

[4] Celia Escamilla-Rivera, A. Hernández-Almada, Miguel A. García-Aspeitia, and V. Motta. Linear perturbations spectra for dynamical dark energy inspired by modified gravity. *arXiv preprint arXiv:2005.13957*.

[5] N. M. Jiménez Cruz and Celia Escamilla-Rivera. Late-time and Big Bang Nucleosynthesis constraints for generic modified gravity

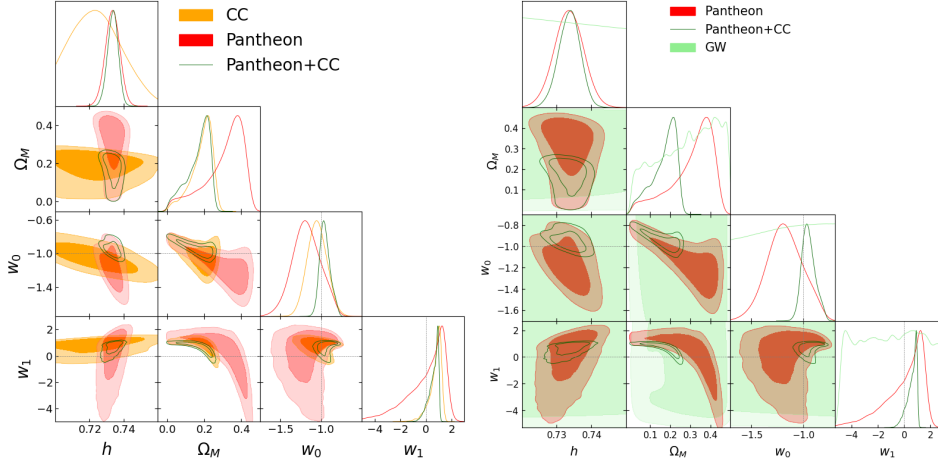


FIG. 9: 1- σ and 2- σ confidence contours for the cosmological parameters h , Ω_m , w_0 and w_1 for the CPL model. *Left:* Analyses performed using Pantheon compilation (red color) and CC data (orange color). *Right:* Analyses performed using Pantheon compilation, CC data and GW catalogues (green color).

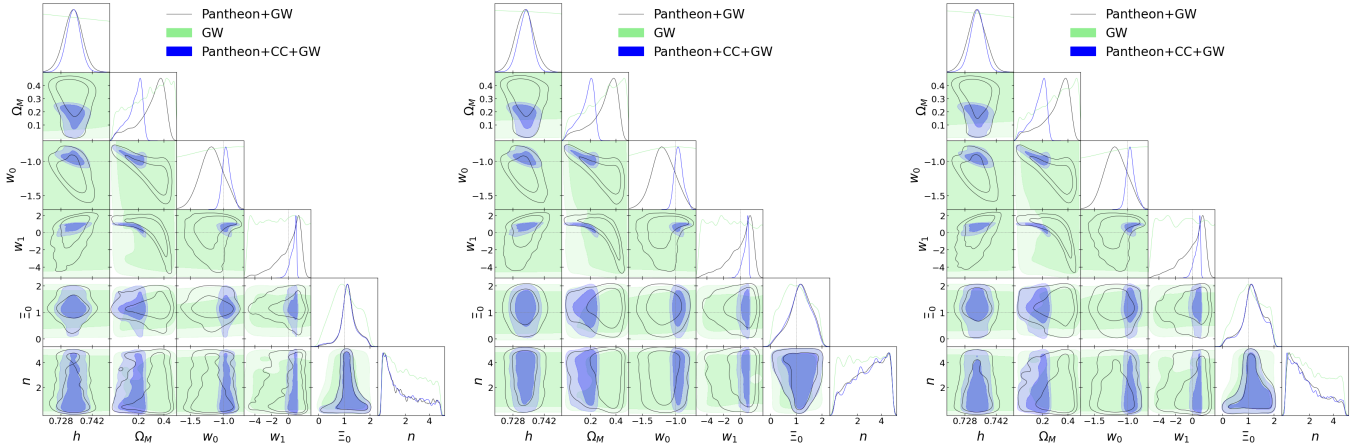


FIG. 10: 1- σ and 2- σ confidence contours for the cosmological parameters in CPL h , Ω_m , w_0 , w_1 , Ξ_0 and n using the combinations of samples: Pantheon+GW (black color), GW catalogues (green color) and Pantheon+CC+GW (blue color). *Left:* case with δ_1 , *middle:* case with δ_2 and *right:* case with δ_3 .

surveys. *Eur. Phys. J. Plus*, 136(1):51, 2021.

[6] Sudipta Das, Abdulla Al Mamon, and Manisha Banerjee. A new parametrization of dark energy equation of state leading to double exponential potential. *Res. Astron. Astrophys.*, 18(11):131, 2018.

[7] Emilio Elizalde, Martiros Khurshudyan, and Shin'ichi Nojiri. Cosmological singularities in interacting dark energy models with an $\omega(q)$ parametrization. *Int. J. Mod. Phys. D*, 28(01):1950019, 2018.

[8] Mehdi Rezaei, Mohammad Malekjani, Spyros Basilakos, Ahmad Mehrabi, and David F. Mota. Constraints to Dark Energy Using PADE Parameterizations. *Astrophys. J.*, 843(1):65, 2017.

[9] Celia Escamilla-Rivera and Salvatore Capozziello. Unveiling cosmography from the dark energy equation of state. *Int. J. Mod. Phys. D*, 28(12):1950154, 2019.

[10] Cristian Zamora Muñoz and Celia Escamilla-Rivera. Inverse Cosmography: testing the effectiveness of cosmographic polynomials using machine learning. *JCAP*, 12:007, 2020.

[11] Eleonora Di Valentino, Luis A Anchordoqui, Yacine Ali-Haimoud, Luca Amendola, Nikki Arendse, Marika Asgari, Mario Ballardini, Elia Battistelli, Micol Benetti, Simon Birrer, et al. Cosmology intertwined i: Perspectives for the next decade. *arXiv preprint arXiv:2008.11283*, 2020.

[12] B. P. Abbott et al. Multi-messenger Observations of a Binary Neutron Star Merger. *Astrophys. J. Lett.*, 848(2):L12, 2017.

[13] Jose María Ezquiaga and Miguel Zumalacárregui. Dark Energy in light of Multi-Messenger Gravitational-Wave astronomy. *Front. Astron. Space Sci.*, 5:44, 2018.

[14] Lorenzo Bordin, Edmund J. Copeland, and Antonio Padilla. Dark energy loopholes some time after GW170817. *JCAP*, 11:063, 2020.

[15] B. P. Abbott et al. GWTC-1: A Gravitational-Wave Transient Catalog of Compact Binary Mergers Observed by LIGO and Virgo during

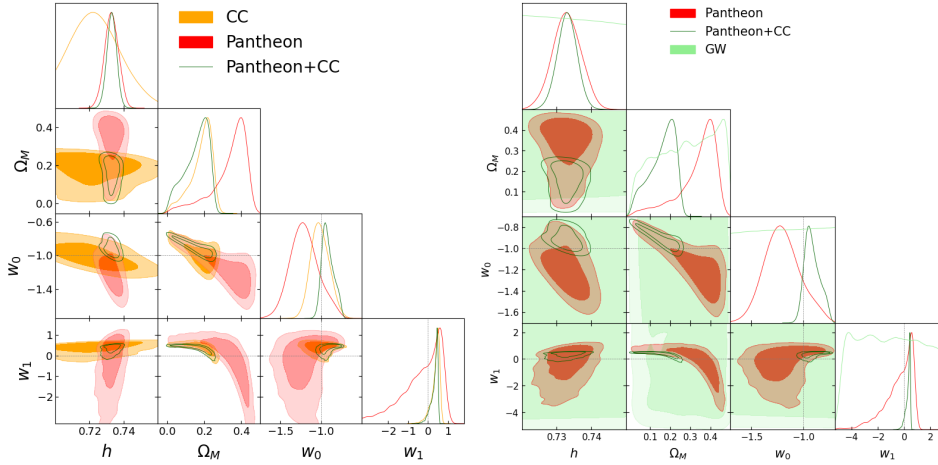


FIG. 11: 1- σ and 2- σ confidence contours for the cosmological parameters h , Ω_m , w_0 and w_1 for the BA model. *Left:* Analyses performed using Pantheon compilation (red color) and CC data (orange color). *Right:* Analyses performed using Pantheon compilation, CC data and GW catalogues (green color).

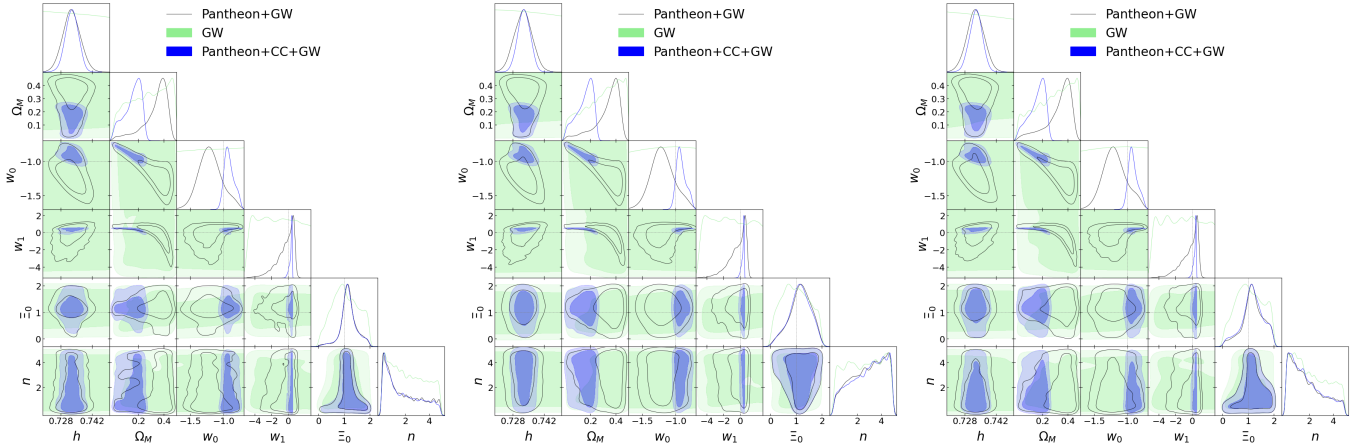


FIG. 12: 1- σ and 2- σ confidence contours for the cosmological parameters in BA h , Ω_m , w_0 , w_1 , Ξ_0 and n using the combinations of samples: Pantheon+GW (black color), GW catalogues (green color) and Pantheon+CC+GW (blue color). *Left:* case with δ_1 , *middle:* case with δ_2 and *right:* case with δ_3 .

the First and Second Observing Runs. *Phys. Rev. X*, 9(3):031040, 2019.

[16] Michel Chevallier and David Polarski. Accelerating universes with scaling dark matter. *Int. J. Mod. Phys. D*, 10:213–224, 2001.

[17] Yun Wang. Figure of merit for dark energy constraints from current observational data. *Physical Review D*, 77(12):123525, 2008.

[18] David W Hogg. Distance measures in cosmology. *arXiv preprint astro-ph/9905116*, 1999.

[19] S. Weinberg and W. Steven. *Gravitation and Cosmology: Principles and Applications of the General Theory of Relativity*. Wiley, 1972.

[20] Scott Dodelson and Fabian Schmidt. *Modern Cosmology*. Academic Press, 2020.

[21] Bernard Schutz. *A first course in general relativity*. Cambridge university press, 2009.

[22] Sanjeev Dhurandhar and Bangalore Sathyaprakash. Cosmic sirens: discovery of gravitational waves and their impact on astrophysics and fundamental physics. *Current Science*, 113(4):663–671, 2017.

[23] Thibault Damour. Gravitational waves and binary black holes. *Ondes Gravitationnelles, Séminaire Poincaré*, 22:1–51, 2016.

[24] Benjamin P Abbott, Richard Abbott, TD Abbott, MR Abernathy, Fausto Acernese, Kendall Ackley, Carl Adams, Thomas Adams, Paolo Addesso, RX Adhikari, et al. Observation of gravitational waves from a binary black hole merger. *Physical review letters*, 116(6):061102, 2016.

[25] Ayan Mitra, Jurgen Mifsud, David F. Mota, and David Parkinson. Cosmology with the Einstein Telescope: No Slip Gravity Model and Redshift Specifications. *arXiv preprint arXiv:2010.00189*.

[26] Enis Belgacem, Gianluca Calcagni, Marco Crisostomi, Charles Dalang, Yves Dirian, Jose María Ezquiaga, Matteo Fasiello, Stefano Foffa, Alexander Ganz, Juan García-Bellido, et al. Testing modified gravity at cosmological distances with lisa standard sirens. *Journal of Cosmology and Astroparticle Physics*, 2019(07):024, 2019.

[27] Steven Weinberg. The Cosmological constant problems. In *4th ISSDDM (DM 2000)*, pages 18–26, 2 2000.

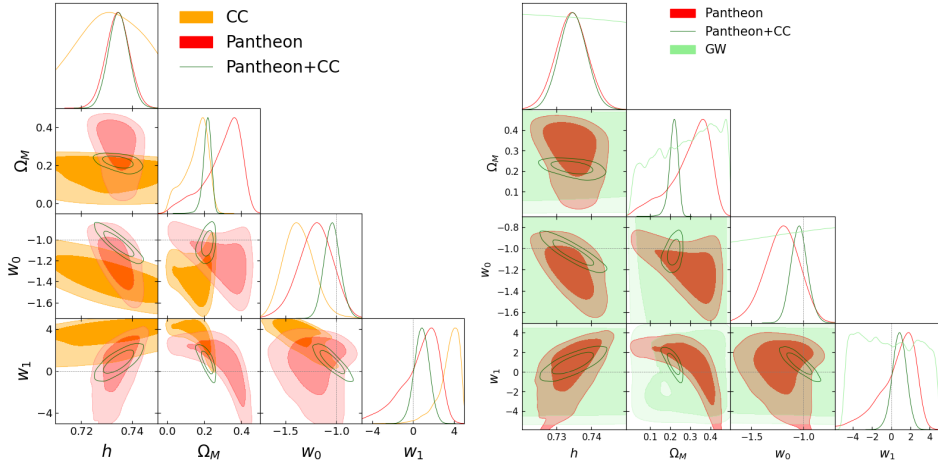


FIG. 13: 1- σ and 2- σ confidence contours for the cosmological parameters h , Ω_m , w_0 and w_1 for the JBP model. *Left:* Analyses performed using Pantheon compilation (red color) and CC data (orange color). *Right:* Analyses performed using Pantheon compilation, CC data and GW catalogues (green color).

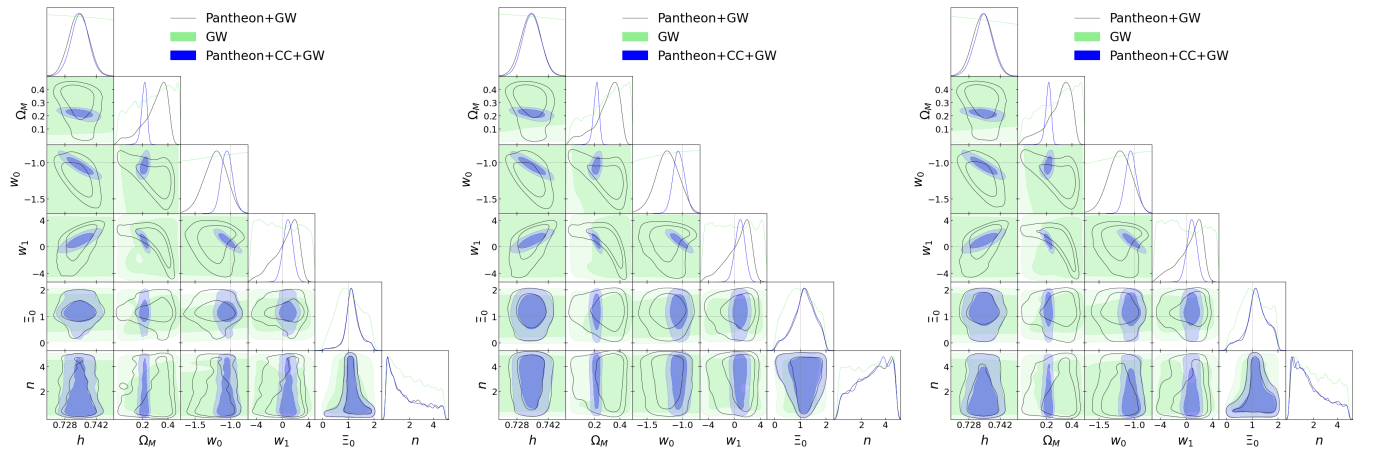


FIG. 14: 1- σ and 2- σ confidence contours for the cosmological parameters in JBP h , Ω_m , w_0 , w_1 , Ξ_0 and n using the combinations of samples: Pantheon+GW (black color), GW catalogues (green color) and Pantheon+CC+GW (blue color). *Left:* case with δ_1 , *middle:* case with δ_2 and *right:* case with δ_3 .

- [28] Timothy Clifton, Pedro G. Ferreira, Antonio Padilla, and Constantinos Skordis. Modified Gravity and Cosmology. *Phys. Rept.*, 513:1–189, 2012.
- [29] Eric V. Linder. The Dynamics of Quintessence, The Quintessence of Dynamics. *Gen. Rel. Grav.*, 40:329–356, 2008.
- [30] EM Barboza Jr and JS Alcaniz. A parametric model for dark energy. *Physics Letters B*, 666(5):415–419, 2008.
- [31] HK Jassal, JS Bagla, and T Padmanabhan. Wmap constraints on low redshift evolution of dark energy. *Monthly Notices of the Royal Astronomical Society: Letters*, 356(1):L11–L16, 2005.
- [32] Dragan Huterer and Michael S. Turner. Probing dark energy: Methods and strategies. *Phys. Rev. D*, 64:123527, Nov 2001.
- [33] Christof Wetterich. Phenomenological parameterization of quintessence. *Physics Letters B*, 594(1-2):17–22, 2004.
- [34] Daniel Moshe Scolnic, DO Jones, A Rest, YC Pan, R Chornock, RJ Foley, ME Huber, R Kessler, Gautham Narayan, AG Riess, et al. The complete light-curve sample of spectroscopically confirmed sne ia from pan-starrs1 and cosmological constraints from the combined pantheon sample. *The Astrophysical Journal*, 859(2):101, 2018.
- [35] David W Hogg, Jo Bovy, and Dustin Lang. Data analysis recipes: Fitting a model to data. *arXiv preprint arXiv:1008.4686*, 2010.
- [36] Juan Magaña, Mario H Amante, Miguel A Garcia-Aspeitia, and V Motta. The Cardassian expansion revisited: constraints from updated Hubble parameter measurements and type Ia supernova data. *Monthly Notices of the Royal Astronomical Society*, 476(1):1036–1049, 02 2018.
- [37] BP Abbott, Richard Abbott, TD Abbott, S Abraham, F Acernese, K Ackley, C Adams, RX Adhikari, VB Adya, C Affeldt, et al. Gwtc-1: a gravitational-wave transient catalog of compact binary mergers observed by ligo and virgo during the first and second observing runs. *Physical Review X*, 9(3):031040, 2019.
- [38] R Abbott, TD Abbott, S Abraham, F Acernese, K Ackley, A Adams, C Adams, RX Adhikari, VB Adya, C Affeldt, et al. Gwtc-2: Compact

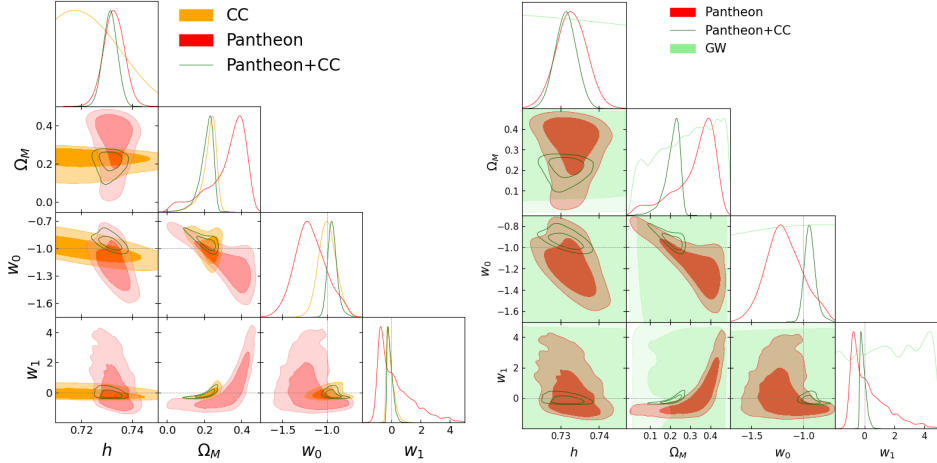


FIG. 15: 1- σ and 2- σ confidence contours for the cosmological parameters h , Ω_M , w_0 and w_1 for the LR model. *Left*: Analyses performed using Pantheon compilation (red color) and CC data (orange color). *Right*: Analyses performed using Pantheon compilation, CC data and GW catalogues (green color).

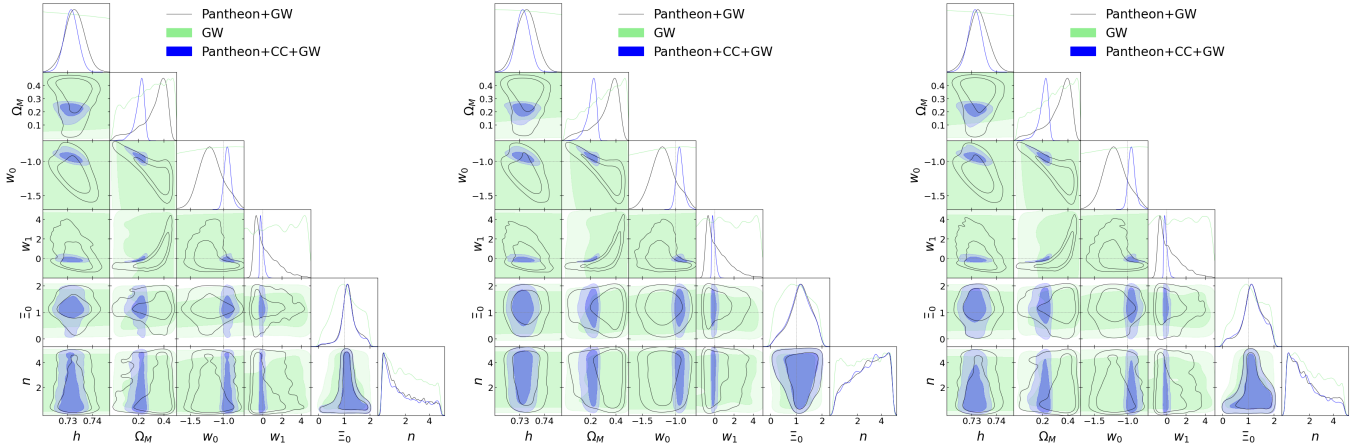


FIG. 16: 1- σ and 2- σ confidence contours for the cosmological parameters in LR h , Ω_M , w_0 , w_1 , Ξ_0 and n using the combinations of samples: Pantheon+GW (black color), GW catalogues (green color) and Pantheon+CC+GW (blue color). *Left*: case with δ_1 , *middle*: case with δ_2 and *right*: case with δ_3 .

binary coalescences observed by ligo and virgo during the first half of the third observing run. [arXiv preprint arXiv:2010.14527](https://arxiv.org/abs/2010.14527), 2020.

[39] Daniel Foreman-Mackey, David W Hogg, Dustin Lang, and Jonathan Goodman. emcee: the mcmc hammer. *Publications of the Astronomical Society of the Pacific*, 125(925):306, 2013.

[40] Antony Lewis. Getdist: a python package for analysing monte carlo samples. [arXiv preprint arXiv:1910.13970](https://arxiv.org/abs/1910.13970), 2019.

[41] Benjamin Audren, Julien Lesgourges, Karim Benabed, and Simon Prunet. Conservative Constraints on Early Cosmology: an illustration of the Monte Python cosmological parameter inference code. *JCAP*, 02:001, 2013.

[42] Thejs Brinckmann and Julien Lesgourges. MontePython 3: boosted MCMC sampler and other features. *Phys. Dark Univ.*, 24:100260, 2019.

[43] Andrew Gelman and Donald B. Rubin. Inference from Iterative Simulation Using Multiple Sequences. *Statist. Sci.*, 7:457–472, 1992.

[44] Harold Jeffreys. *The Theory of Probability*. Oxford Classic Texts in the Physical Sciences. 1939.

[45] Alan Heavens, Yabebal Fantaye, Arrykrishna Mootoovaloo, Hans Eggers, Zafirah Hosenie, Steve Kroon, and Elena Sellentin. Marginal Likelihoods from Monte Carlo Markov Chains. [arXiv preprint 1704.03472](https://arxiv.org/abs/1704.03472).

[46] Andrew R. Liddle. How many cosmological parameters? *Mon. Not. Roy. Astron. Soc.*, 351:L49–L53, 2004.

[47] Robert E. Kass and Adrian E. Raftery. Bayes factors. *Journal of the American Statistical Association*, 90(430):773–795, 1995.

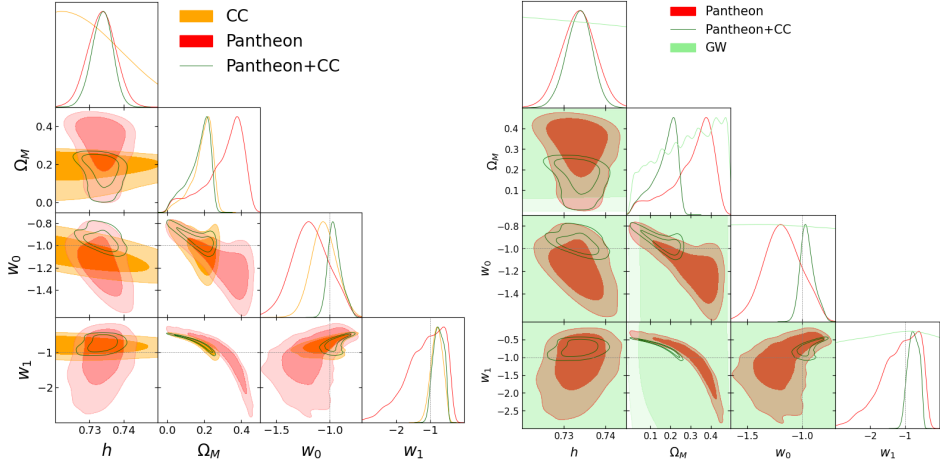


FIG. 17: 1- σ and 2- σ confidence contours for the cosmological parameters h , Ω_m , w_0 and w_1 for the LC model. *Left:* Analyses performed using Pantheon compilation (red color) and CC data (orange color). *Right:* Analyses performed using Pantheon compilation, CC data and GW catalogues (green color).

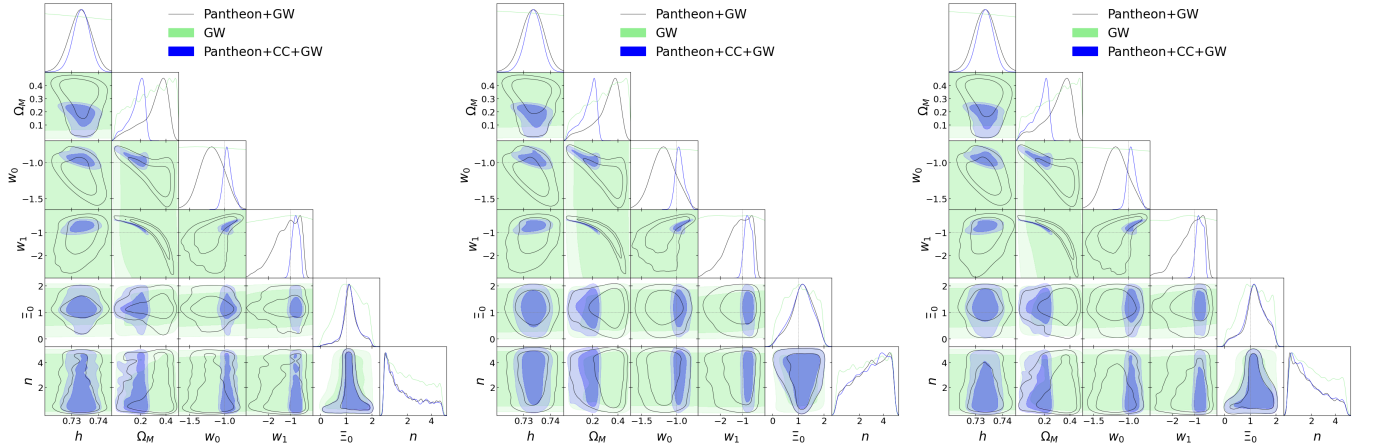


FIG. 18: 1- σ and 2- σ confidence contours for the cosmological parameters in LC h , Ω_m , w_0 , w_1 , Ξ_0 and n using the combinations of samples: Pantheon+GW (black color), GW catalogues (green color) and Pantheon+CC+GW (blue color). *Left:* case with δ_1 , *middle:* case with δ_2 and *right:* case with δ_3 .

Appendix A: Derivation of the tensor for Gravitational Waves

We can compute the h_{ij} (the spacial part of $h_{\mu\nu}$) tensor using the spatial part of the wave equation for GWs [21]

$$\left(\frac{1}{c^2} \frac{\partial^2}{\partial t^2} - \nabla^2 \right) h_{\mu\nu} = \frac{16\pi G}{c^4} T_{\mu\nu}. \quad (\text{A1})$$

To achieve this, it is easier to work with the Green's function. The Green's function equation for this can be expressed as

$$\left(\frac{1}{c^2} \frac{\partial^2}{\partial t^2} - \nabla^2 \right) G(\mathbf{x}, \mathbf{x}_0, t, t_0) = \delta(\mathbf{x} - \mathbf{x}_0) \delta(t - t_0). \quad (\text{A2})$$

By writing the Fourier transform of the Green's function and the Dirac's deltas, and solving the equation the Green's function is

$$G(\mathbf{x}, \mathbf{x}_0, t, t_0) = \frac{\delta \left(t - t_0 - \frac{|\mathbf{x} - \mathbf{x}_0|}{c} \right)}{4\pi |\mathbf{x} - \mathbf{x}_0|}, \quad (\text{A3})$$

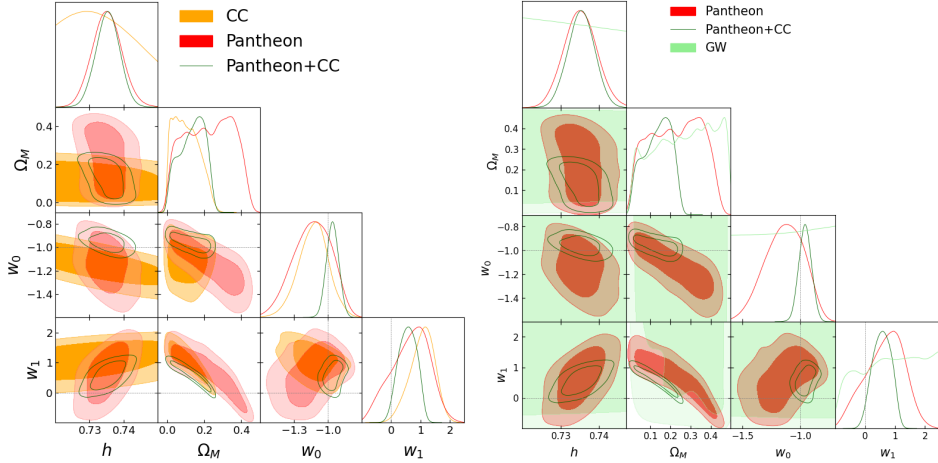


FIG. 19: 1- σ and 2- σ confidence contours for the cosmological parameters h , Ω_m , w_0 and w_1 for the WP model. *Left*: Analyses performed using Pantheon compilation (red color) and CC data (orange color). *Right*: Analyses performed using Pantheon compilation, CC data and GW catalogues (green color).

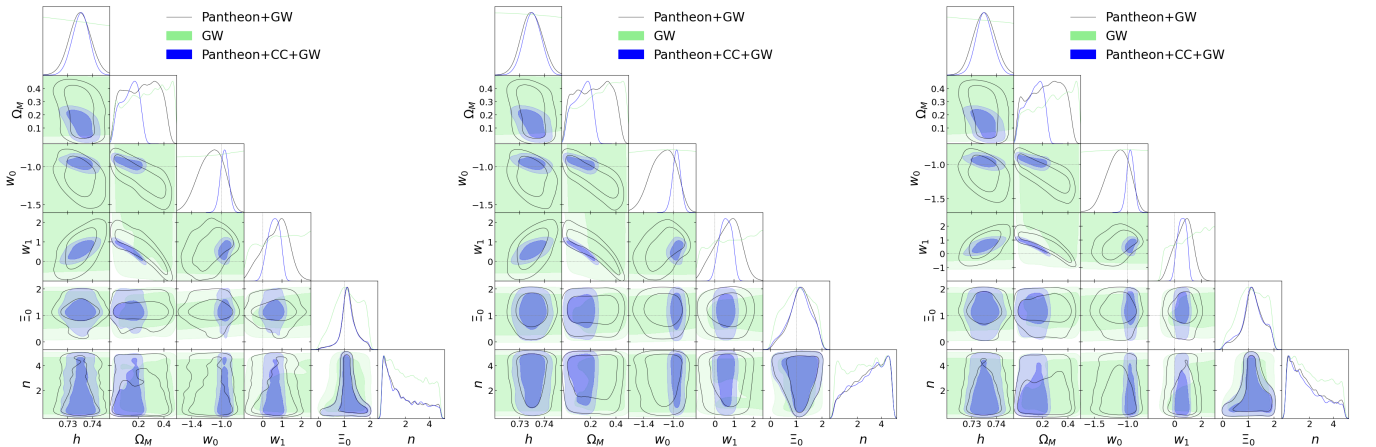


FIG. 20: 1- σ and 2- σ confidence contours for the cosmological parameters in WP h , Ω_m , w_0 , w_1 , Ξ_0 and n using the combinations of samples: Pantheon+GW (black color), GW catalogues (green color) and Pantheon+CC+GW (blue color). *Left*: case with δ_1 , *middle*: case with δ_2 and *right*: case with δ_3 .

then, we can obtain the following solution (here we only focus on the spacial part of the solution)

$$h_{ij}^{TT} = \frac{16\pi G}{c^4} \int_V d^3x_0 dt_0 T_{ij}(\mathbf{x}_0, t_0) \frac{\delta\left(t - t_0 - \frac{|\mathbf{x} - \mathbf{x}_0|}{c}\right)}{4\pi|\mathbf{x} - \mathbf{x}_0|}, \quad (\text{A4})$$

by integrating over t_0

$$h_{ij}^{TT} = \frac{4G}{c^4} \int_V d^3x_0 \frac{T_{ij}\left(t - \frac{|\mathbf{x} - \mathbf{x}_0|}{c}, \mathbf{x}_0\right)}{|\mathbf{x} - \mathbf{x}_0|}. \quad (\text{A5})$$

If the system is far away then $|\mathbf{x} - \mathbf{x}_0| \approx D_S$, where D_S is the siren distance to the source (the distance associated with the GW is the siren distance), then

$$h_{ij}^{TT} = \frac{4G}{c^4 D_S} \int d^3x_0 T_{ij}\left(t - \frac{D_S}{c}, \mathbf{x}_0\right). \quad (\text{A6})$$

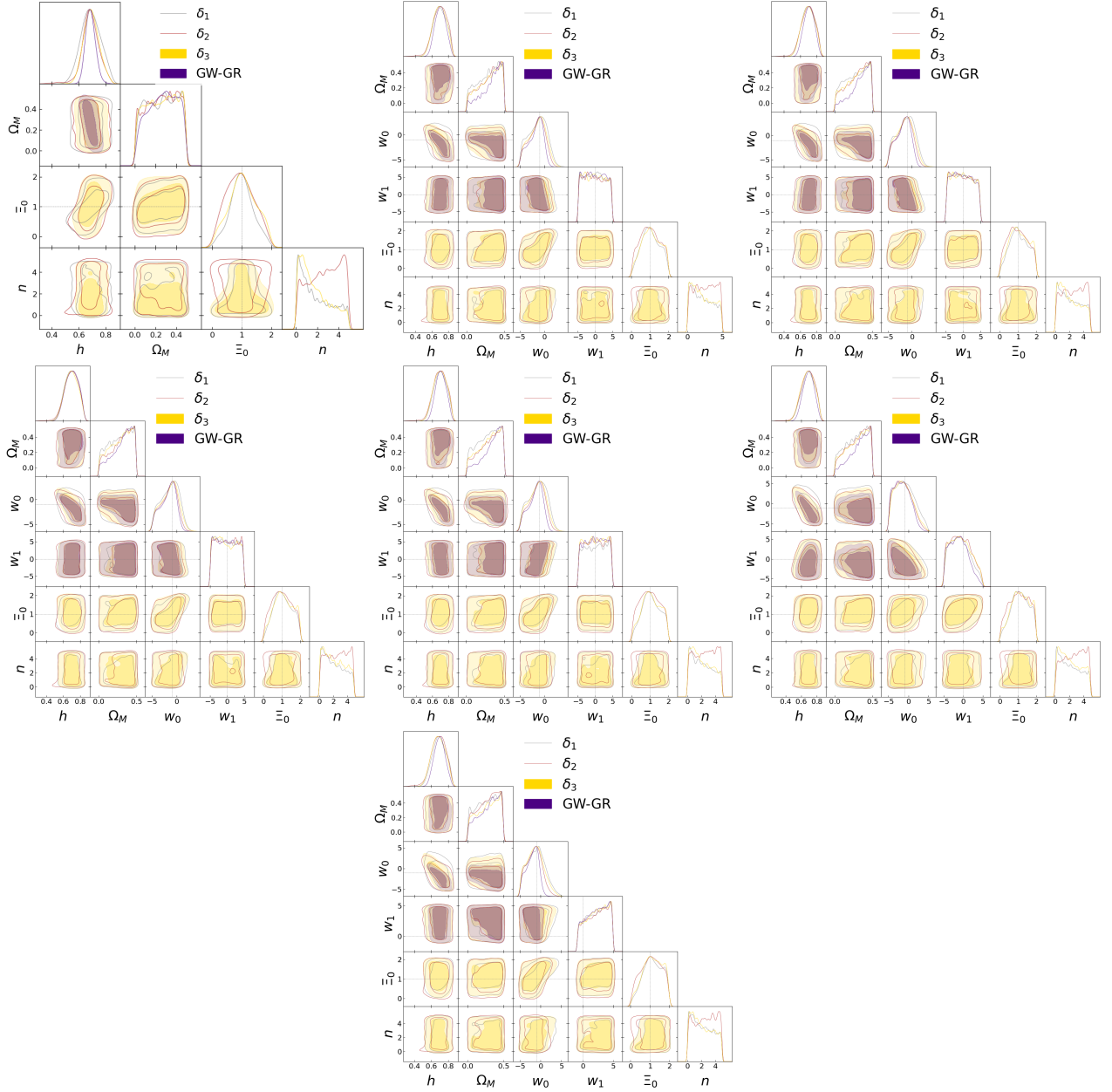


FIG. 21: 1- σ and 2- σ confidence contours for the cosmological parameters h , Ω_M , w_0 , w_1 , Ξ_0 and n for the seven models. The overlapping corresponds to the three delta functions plus the GR case. From bottom left up to bottom: Λ CDM, CPL, BA, JBP, LR, LC and WP, respectively.

Due to the gauge condition $\partial_\nu T^{\mu\nu} = 0$ [21], the expressions $\partial T^{\mu 0}/\partial t = -\partial T^{\mu i}/\partial x^i$ and $\partial T^{00}/\partial t = -\partial T^{0i}/\partial x^i$ hold. By using these expressions and the conditions under the source is far away (the surface integrals that include the stress-energy tensor are equal to zero) and slow-motion ($\partial x^i/\partial t \approx 0$) holds then the following expressions can be derived

$$\int d^3x T_{ij} = \frac{1}{2} \frac{d}{dt} \int d^3x (T_{i0}x_j + T_{j0}x_i), \quad (\text{A7})$$

$$\int d^3x (T_{i0}x_j + T_{j0}x_i) = \frac{d}{dt} \int d^3x T_{00}x_i x_j. \quad (\text{A8})$$

These are obtained by applying integration by parts in the right side above expressions and consider zero over some terms with the conditions explained in the previous paragraph. Then by defining the quadrupole moment tensor by $I_{ij} = \int d^3x \rho(\mathbf{x}) x_i x_j$

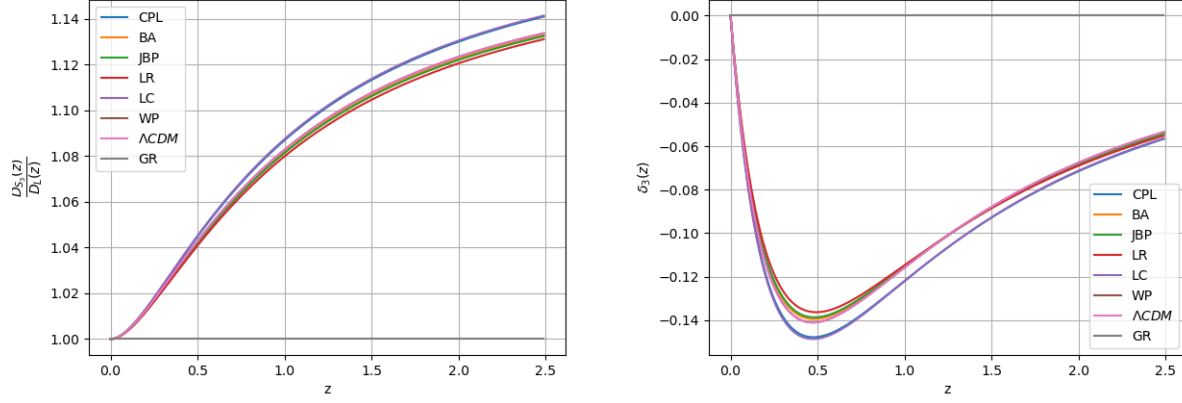


FIG. 22: *Left:* Siren distance-luminosity distance ratio for the Λ CDM model and the six dark energy parameterisations with the δ_3 function with the Ξ_0 and n best fits. The GR case is also plotted to compare with the other models. *Right:* δ_3 function for the Λ CDM model and the six dark energy parameterisations with the δ_3 function with the Ξ_0 and n best fits. The GR case is also plotted to compare with the other models.

Model	Database	h	Ω_M	w_0	w_1
Λ CDM	CC	0.7152 ± 0.0099	0.248 ± 0.014	-	-
	Pantheon	0.7284 ± 0.0023	0.285 ± 0.013	-	-
	Pantheon+CC	0.7330 ± 0.0020	0.2447 ± 0.0073	-	-
CPL	CC	0.722 ± 0.017	$0.186^{+0.071}_{-0.032}$	-1.05 ± 0.12	$0.77^{+0.54}_{-0.21}$
	Pantheon	0.7335 ± 0.0042	$0.306^{+0.13}_{-0.044}$	-1.18 ± 0.17	$-0.05^{+1.9}_{-0.61}$
	Pantheon+CC	0.7337 ± 0.0031	$0.168^{+0.078}_{-0.031}$	$-0.950^{+0.053}_{-0.074}$	$0.61^{+0.46}_{-0.17}$
BA	CC	0.722 ± 0.016	$0.184^{+0.073}_{-0.031}$	$-1.01^{+0.10}_{-0.12}$	$0.380^{+0.25}_{-0.090}$
	Pantheon	0.7329 ± 0.0041	$0.336^{+0.11}_{-0.034}$	$-1.20^{+0.15}_{-0.19}$	$-0.40^{+1.3}_{-0.43}$
	Pantheon+CC	0.7330 ± 0.0029	$0.159^{+0.085}_{-0.038}$	$-0.915^{+0.057}_{-0.090}$	$0.326^{+0.20}_{-0.061}$
JBP	CC	$0.732^{+0.017}_{-0.015}$	$0.156^{+0.081}_{-0.038}$	$-1.37^{+0.14}_{-0.16}$	$3.51^{+1.3}_{-0.42}$
	Pantheon	0.7344 ± 0.0045	$0.299^{+0.12}_{-0.051}$	$-1.21^{+0.18}_{-0.16}$	$0.49^{+2.5}_{-0.97}$
	Pantheon+CC	0.7347 ± 0.0039	$0.217^{+0.024}_{-0.018}$	-1.041 ± 0.079	0.86 ± 0.73
LR	CC	0.718 ± 0.016	$0.226^{+0.046}_{-0.020}$	$-0.992^{+0.094}_{-0.11}$	$-0.09^{+0.12}_{-0.31}$
	Pantheon	0.7328 ± 0.0040	$0.324^{+0.12}_{-0.039}$	$-1.18^{+0.16}_{-0.19}$	$0.37^{+0.43}_{-1.5}$
	Pantheon+CC	0.7314 ± 0.0028	$0.211^{+0.044}_{-0.020}$	$-0.936^{+0.043}_{-0.058}$	$-0.096^{+0.095}_{-0.24}$
LC	CC	0.723 ± 0.016	$0.188^{+0.070}_{-0.028}$	-1.05 ± 0.12	$-0.80^{+0.19}_{-0.16}$
	Pantheon	0.7336 ± 0.0041	$0.304^{+0.13}_{-0.047}$	-1.18 ± 0.17	$-1.18^{+0.75}_{-0.31}$
	Pantheon+CC	$0.7337^{+0.0032}_{-0.0029}$	$0.170^{+0.078}_{-0.031}$	$-0.952^{+0.050}_{-0.074}$	$-0.75^{+0.19}_{-0.15}$
WP	Chronometers	0.729 ± 0.017	$0.105^{+0.044}_{-0.095}$	$-1.13^{+0.14}_{-0.12}$	$1.07^{+0.48}_{-0.36}$
	Pantheon	0.7352 ± 0.0043	$0.22^{+0.16}_{-0.14}$	$-1.14^{+0.19}_{-0.15}$	$0.66^{+0.77}_{-0.54}$
	Pantheon+CC	0.7354 ± 0.0035	$0.135^{+0.090}_{-0.050}$	-0.959 ± 0.054	$0.57^{+0.34}_{-0.31}$

TABLE II: Best fit values for the four cosmological parameters with their one- σ uncertainties. The best fit values are reported for the standard model Λ CDM and the six dynamical dark energy parameterisations. The second column indicates the database used.

the final expression is

$$h_{ij} = \frac{2G}{c^4 D_S} \left[\frac{d^2 I_{ij} \left(t - \frac{R}{c} \right)}{dt^2} \right]^{TT}, \quad (\text{A9})$$

where TT denotes that is the transverse and traceless part of I_{ij} .

Model	Database (using δ_1)	h	Ω_M	w_0	w_1	Ξ_0	n
Λ CDM	GW	0.690 ± 0.073	0.26 ± 0.14	-	-	1.00 ± 0.40	$1.93^{+0.77}_{-1.9}$
	Pantheon+GW	0.7283 ± 0.0023	0.286 ± 0.013	-	-	$1.19^{+0.24}_{-0.30}$	$1.8^{+1.2}_{-1.8}$
	Pantheon+CC+GW	0.7331 ± 0.0019	0.2447 ± 0.0072	-	-	$1.17^{+0.25}_{-0.28}$	$1.7^{+1.2}_{-1.7}$
CPL	GW	0.698 ± 0.078	$0.286^{+0.21}_{-0.079}$	$-1.4^{+2.2}_{-1.7}$	$-0.1^{+2.9}_{-4.6}$	$1.04^{+0.48}_{-0.57}$	$2.2^{+1.5}_{-2.1}$
	Pantheon+GW	0.7335 ± 0.0041	$0.301^{+0.13}_{-0.046}$	-1.18 ± 0.17	$0.08^{+1.7}_{-0.62}$	$1.18^{+0.24}_{-0.30}$	$1.8^{+1.1}_{-1.8}$
	Pantheon+CC+GW	0.7337 ± 0.0031	$0.169^{+0.077}_{-0.030}$	$-0.951^{+0.054}_{-0.074}$	$0.61^{+0.46}_{-0.18}$	1.16 ± 0.34	$1.75^{+0.98}_{-1.8}$
BA	GW	0.698 ± 0.078	$0.281^{+0.21}_{-0.093}$	$-1.4^{+2.3}_{-1.6}$	$-0.2^{+2.1}_{-4.4}$	$1.06^{+0.51}_{-0.58}$	$2.2^{+1.1}_{-2.2}$
	Pantheon+GW	0.7329 ± 0.0040	$0.332^{+0.11}_{-0.033}$	$-1.20^{+0.15}_{-0.19}$	$-0.34^{+1.3}_{-0.42}$	$1.18^{+0.25}_{-0.29}$	$1.8^{+1.6}_{-1.8}$
	Pantheon+CC+GW	0.7331 ± 0.0029	$0.157^{+0.088}_{-0.037}$	$-0.913^{+0.056}_{-0.092}$	$0.324^{+0.21}_{-0.056}$	$1.17^{+0.24}_{-0.29}$	$1.8^{+1.0}_{-1.8}$
JBP	GW	0.698 ± 0.077	$0.28^{+0.21}_{-0.14}$	$-1.4^{+2.2}_{-1.6}$	$-0.1^{+3.8}_{-4.5}$	$1.06^{+0.49}_{-0.56}$	$2.17^{+0.87}_{-2.1}$
	Pantheon+GW	0.7344 ± 0.0044	$0.299^{+0.12}_{-0.044}$	$-1.21^{+0.17}_{-0.15}$	$0.6^{+2.3}_{-1.0}$	$1.18^{+0.24}_{-0.28}$	$1.8^{+1.1}_{-1.8}$
	Pantheon+CC+GW	0.7348 ± 0.0040	$0.216^{+0.024}_{-0.018}$	$-1.043^{+0.074}_{-0.083}$	0.89 ± 0.74	$1.17^{+0.24}_{-0.29}$	$1.77^{+0.69}_{-1.8}$
LR	GW	$0.698^{+0.085}_{-0.075}$	$0.282^{+0.21}_{-0.092}$	$-1.4^{+2.3}_{-1.6}$	0.2 ± 2.9	1.07 ± 0.49	$2.2^{+1.2}_{-2.1}$
	Pantheon+GW	0.7328 ± 0.0040	$0.324^{+0.12}_{-0.034}$	$-1.18^{+0.15}_{-0.20}$	$0.33^{+0.48}_{-1.4}$	$1.17^{+0.25}_{-0.30}$	$1.75^{+0.69}_{-1.8}$
	Pantheon+CC+GW	0.7314 ± 0.0028	$0.211^{+0.043}_{-0.020}$	$-0.937^{+0.044}_{-0.056}$	$-0.098^{+0.095}_{-0.24}$	$1.16^{+0.25}_{-0.28}$	$1.77^{+0.94}_{-1.8}$
LC	GW	$0.691^{+0.098}_{-0.077}$	$0.28^{+0.21}_{-0.13}$	$-0.9^{+1.7}_{-3.3}$	$-0.8^{+1.8}_{-3.4}$	1.12 ± 0.48	$2.18^{+0.88}_{-2.1}$
	Pantheon+GW	0.7333 ± 0.0042	$0.309^{+0.13}_{-0.044}$	-1.18 ± 0.17	$-1.21^{+0.77}_{-0.32}$	$1.17^{+0.25}_{-0.29}$	$1.8^{+1.4}_{-1.8}$
	Pantheon+CC+GW	0.7337 ± 0.0031	$0.172^{+0.075}_{-0.029}$	$-0.953^{+0.051}_{-0.069}$	$-0.75^{+0.18}_{-0.15}$	$1.17^{+0.26}_{-0.29}$	$1.74^{+0.61}_{-1.8}$
WP	GW	0.695 ± 0.079	$0.27^{+0.22}_{-0.12}$	-1.1 ± 2.1	$2.3^{+2.6}_{-1.7}$	$1.14^{+0.68}_{-0.44}$	$2.2^{+1.6}_{-2.0}$
	Pantheon+GW	0.7351 ± 0.0044	0.22 ± 0.12	$-1.14^{+0.19}_{-0.15}$	$0.67^{+0.76}_{-0.58}$	1.17 ± 0.33	$1.8^{+1.0}_{-1.8}$
	Pantheon+CC+GW	0.7353 ± 0.0034	$0.134^{+0.086}_{-0.056}$	-0.958 ± 0.054	$0.58^{+0.36}_{-0.28}$	$1.17^{+0.25}_{-0.29}$	$1.8^{+1.1}_{-1.8}$

TABLE III: Best fit values for the seven cosmological models discussed in Sec.4 at $1-\sigma$ uncertainties. In this case we consider the GW catalogues using δ_1 function (23).

Model	Database (using δ_2)	h	Ω_M	w_0	w_1	Ξ_0	n
Λ CDM	GW	0.686 ± 0.067	$0.26^{+0.22}_{-0.15}$	-	-	$0.95^{+0.44}_{-0.56}$	$2.72^{+2.2}_{-0.92}$
	Pantheon+GW	0.7283 ± 0.0023	0.286 ± 0.013	-	-	$1.16^{+0.49}_{-0.35}$	$2.92^{+2.0}_{-0.81}$
	Pantheon+CC+GW	0.7330 ± 0.0019	0.2446 ± 0.0072	-	-	$1.14^{+0.55}_{-0.35}$	$2.93^{+2.0}_{-0.81}$
CPL	GW	$0.696^{+0.095}_{-0.077}$	$0.30^{+0.19}_{-0.11}$	$-1.6^{+2.0}_{-1.4}$	-0.1 ± 2.9	1.01 ± 0.52	2.6 ± 1.4
	Pantheon+GW	0.7334 ± 0.0042	$0.307^{+0.13}_{-0.043}$	-1.18 ± 0.17	$-0.01^{+1.8}_{-0.71}$	$1.17^{+0.50}_{-0.36}$	$2.91^{+2.0}_{-0.83}$
	Pantheon+CC+GW	0.7337 ± 0.0031	$0.167^{+0.079}_{-0.033}$	$-0.949^{+0.053}_{-0.075}$	$0.62^{+0.45}_{-0.16}$	$1.13^{+0.51}_{-0.36}$	$2.96^{+1.9}_{-0.88}$
BA	GW	$0.695^{+0.096}_{-0.073}$	$0.297^{+0.20}_{-0.076}$	$-1.6^{+2.0}_{-1.4}$	$-0.1^{+2.6}_{-4.4}$	$0.99^{+0.52}_{-0.63}$	2.6 ± 1.4
	Pantheon+GW	0.7327 ± 0.0041	$0.331^{+0.12}_{-0.033}$	$-1.19^{+0.15}_{-0.19}$	$-0.36^{+1.3}_{-0.44}$	$1.16^{+0.51}_{-0.35}$	$2.89^{+2.0}_{-0.85}$
	Pantheon+CC+GW	0.7331 ± 0.0028	$0.157^{+0.086}_{-0.037}$	$-0.914^{+0.052}_{-0.091}$	$0.332^{+0.20}_{-0.062}$	$1.14^{+0.48}_{-0.36}$	$2.93^{+2.0}_{-0.79}$
JBP	GW	$0.696^{+0.093}_{-0.072}$	$0.299^{+0.19}_{-0.078}$	$-1.6^{+2.0}_{-1.3}$	0.0 ± 2.9	1.01 ± 0.51	2.6 ± 1.5
	Pantheon+GW	0.7344 ± 0.0044	$0.296^{+0.12}_{-0.043}$	-1.21 ± 0.16	$0.6^{+2.3}_{-1.1}$	$1.17^{+0.50}_{-0.36}$	$2.91^{+2.0}_{-0.83}$
	Pantheon+CC+GW	0.7349 ± 0.0040	$0.216^{+0.024}_{-0.018}$	-1.045 ± 0.080	0.89 ± 0.74	$1.14^{+0.49}_{-0.38}$	$2.9^{+2.0}_{-1.1}$
LR	GW	$0.693^{+0.094}_{-0.077}$	$0.298^{+0.19}_{-0.074}$	$-1.6^{+2.0}_{-1.4}$	0.1 ± 2.9	0.997 ± 0.53	2.6 ± 1.5
	Pantheon+GW	0.7327 ± 0.0040	$0.323^{+0.12}_{-0.037}$	$-1.18^{+0.16}_{-0.20}$	$0.33^{+0.47}_{-1.4}$	$1.16^{+0.50}_{-0.35}$	$2.91^{+2.0}_{-0.81}$
	Pantheon+CC+GW	0.7313 ± 0.0028	$0.210^{+0.045}_{-0.019}$	$-0.935^{+0.044}_{-0.058}$	$-0.101^{+0.094}_{-0.23}$	$1.15^{+0.50}_{-0.38}$	$2.9^{+2.0}_{-1.0}$
LC	GW	$0.687^{+0.10}_{-0.076}$	$0.294^{+0.20}_{-0.092}$	$-1.4^{+1.6}_{-2.9}$	$-0.6^{+2.2}_{-3.8}$	$1.06^{+0.64}_{-0.57}$	$2.7^{+2.2}_{-1.4}$
	Pantheon+GW	0.7334 ± 0.0042	$0.310^{+0.13}_{-0.044}$	-1.18 ± 0.17	$-1.21^{+0.77}_{-0.30}$	$1.15^{+0.51}_{-0.35}$	$2.91^{+2.0}_{-0.79}$
	Pantheon+CC+GW	0.7337 ± 0.0031	$0.168^{+0.079}_{-0.028}$	$-0.950^{+0.050}_{-0.075}$	-0.75 ± 0.15	$1.13^{+0.50}_{-0.39}$	$2.93^{+2.0}_{-0.83}$
WP	GW	$0.687^{+0.093}_{-0.078}$	$0.280^{+0.20}_{-0.088}$	-1.6 ± 1.8	$2.3^{+2.6}_{-1.1}$	$1.06^{+0.68}_{-0.46}$	2.6 ± 1.5
	Pantheon+GW	0.7350 ± 0.0043	$0.22^{+0.17}_{-0.14}$	$-1.14^{+0.19}_{-0.15}$	$0.66^{+0.77}_{-0.57}$	$1.17^{+0.49}_{-0.37}$	$2.95^{+1.9}_{-0.78}$
	Pantheon+CC+GW	0.7352 ± 0.0035	$0.135^{+0.087}_{-0.055}$	-0.957 ± 0.055	$0.57^{+0.36}_{-0.29}$	$1.13^{+0.51}_{-0.39}$	$2.96^{+2.0}_{-0.78}$

TABLE IV: Best fit values for the seven cosmological models discussed in Sec.4 at $1-\sigma$ uncertainties. In this case we consider the GW catalogues using δ_2 function (24).

Model	Database (using δ_3)	h	Ω_M	w_0	w_1	Ξ_0	n
Λ CDM	GW	$0.694^{+0.054}_{-0.061}$	$0.26^{+0.22}_{-0.12}$	-	-	1.04 ± 0.47	$1.81^{+0.59}_{-1.8}$
	Pantheon+GW	0.7283 ± 0.0023	0.286 ± 0.013	-	-	$1.19^{+0.43}_{-0.37}$	$1.85^{+0.61}_{-1.8}$
	Pantheon+CC+GW	0.7330 ± 0.0019	0.2446 ± 0.0071	-	-	$1.17^{+0.47}_{-0.35}$	$1.8^{+1.1}_{-1.8}$
CPL	GW	0.695 ± 0.076	$0.295^{+0.20}_{-0.080}$	$-1.5^{+2.0}_{-1.6}$	-0.1 ± 2.9	1.07 ± 0.50	$2.2^{+2.5}_{-2.2}$
	Pantheon+GW	0.7335 ± 0.0042	$0.304^{+0.13}_{-0.045}$	-1.18 ± 0.17	$0.03^{+1.8}_{-0.68}$	$1.19^{+0.49}_{-0.34}$	$1.78^{+0.59}_{-1.7}$
	Pantheon+CC+GW	0.7336 ± 0.0031	$0.170^{+0.075}_{-0.029}$	$-0.951^{+0.050}_{-0.072}$	$0.60^{+0.46}_{-0.18}$	$1.18^{+0.45}_{-0.38}$	$1.79^{+0.77}_{-1.8}$
BA	GW	0.696 ± 0.077	$0.29^{+0.20}_{-0.11}$	$-1.5^{+2.1}_{-1.7}$	$-0.1^{+2.7}_{-4.5}$	$1.06^{+0.80}_{-0.58}$	$2.1^{+1.3}_{-2.1}$
	Pantheon+GW	0.7328 ± 0.0039	$0.327^{+0.12}_{-0.036}$	$-1.19^{+0.15}_{-0.20}$	$-0.33^{+1.2}_{-0.43}$	$1.19^{+0.47}_{-0.35}$	$1.81^{+0.57}_{-1.8}$
	Pantheon+CC+GW	0.7330 ± 0.0029	$0.160^{+0.083}_{-0.036}$	$-0.916^{+0.053}_{-0.087}$	$0.323^{+0.20}_{-0.075}$	$1.17^{+0.44}_{-0.39}$	$1.78^{+0.57}_{-1.8}$
JBP	GW	0.697 ± 0.076	$0.29^{+0.20}_{-0.12}$	$-1.4^{+2.1}_{-1.6}$	-0.2 ± 2.9	1.08 ± 0.51	2.2 ± 1.4
	Pantheon+GW	0.7344 ± 0.0044	$0.295^{+0.12}_{-0.047}$	-1.20 ± 0.16	$0.60^{+2.4}_{-0.98}$	$1.19^{+0.45}_{-0.38}$	$1.82^{+0.57}_{-1.8}$
	Pantheon+CC+GW	0.7347 ± 0.0040	$0.216^{+0.024}_{-0.017}$	$-1.040^{+0.074}_{-0.085}$	0.87 ± 0.74	$1.17^{+0.48}_{-0.34}$	$1.77^{+0.56}_{-1.8}$
LR	GW	0.697 ± 0.078	$0.294^{+0.20}_{-0.074}$	$-1.5^{+2.1}_{-1.6}$	0.1 ± 2.9	1.07 ± 0.50	$2.16^{+0.95}_{-2.1}$
	Pantheon+GW	0.7328 ± 0.0040	$0.326^{+0.12}_{-0.037}$	$-1.19^{+0.15}_{-0.19}$	$0.36^{+0.49}_{-1.4}$	$1.18^{+0.45}_{-0.37}$	$1.82^{+0.57}_{-1.8}$
	Pantheon+CC+GW	0.7313 ± 0.0028	$0.210^{+0.044}_{-0.019}$	$-0.935^{+0.040}_{-0.060}$	$-0.102^{+0.092}_{-0.23}$	$1.17^{+0.46}_{-0.37}$	$1.74^{+0.52}_{-1.7}$
LC	GW	0.686 ± 0.084	$0.294^{+0.20}_{-0.078}$	$-1.2^{+1.6}_{-3.0}$	$-0.6^{+1.9}_{-3.7}$	1.13 ± 0.50	$2.2^{+2.4}_{-2.1}$
	Pantheon+GW	0.7336 ± 0.0041	$0.305^{+0.13}_{-0.048}$	-1.18 ± 0.17	$-1.19^{+0.77}_{-0.29}$	$1.18^{+0.47}_{-0.33}$	$1.80^{+0.61}_{-1.8}$
	Pantheon+CC+GW	0.7336 ± 0.0030	$0.168^{+0.079}_{-0.032}$	$-0.949^{+0.052}_{-0.075}$	$-0.75^{+0.19}_{-0.15}$	$1.18^{+0.44}_{-0.38}$	$1.80^{+0.61}_{-1.8}$
WP	GW	0.687 ± 0.079	$0.28^{+0.21}_{-0.11}$	$-1.3^{+1.9}_{-2.3}$	$2.3^{+2.5}_{-1.0}$	$1.14^{+0.69}_{-0.43}$	$2.2^{+1.8}_{-2.1}$
	Pantheon+GW	0.7352 ± 0.0044	$0.23^{+0.17}_{-0.10}$	$-1.14^{+0.19}_{-0.15}$	$0.66^{+0.75}_{-0.58}$	$1.19^{+0.43}_{-0.38}$	$1.85^{+0.71}_{-1.8}$
	Pantheon+CC+GW	0.7353 ± 0.0035	$0.135^{+0.090}_{-0.053}$	-0.958 ± 0.054	$0.57^{+0.37}_{-0.30}$	$1.17^{+0.47}_{-0.37}$	$1.80^{+0.59}_{-1.8}$

TABLE V: Best fit values for the seven cosmological models discussed in Sec.4 at $1-\sigma$ uncertainties. In this case we consider the GW catalogues using δ_3 function (25).

Model	χ^2_{\min}	AIC	BIC	Δ AIC	Δ BIC
Λ CDM	1038.15	1046.15	1066.34	-	-
CPL	1035.24	1047.24	1077.52	1.08	11.17
BA	1034.28	1046.28	1076.57	0.12	10.22
JBP	1035.69	1047.69	1077.97	1.53	11.62
LR	1036.42	1048.42	1078.70	2.26	12.35
LC	1035.24	1047.24	1077.52	1.08	11.17
WP	1035.27	1047.27	1077.55	1.11	11.20

TABLE VI: AIC and BIC criteria for the six models dark energy against Λ CDM for δ_1 (23).

Model	χ^2_{\min}	AIC	BIC	Δ AIC	Δ BIC
Λ CDM	1038.66	1046.66	1066.85	-	-
CPL	1035.72	1047.72	1078.01	1.06	11.15
BA	1034.77	1046.77	1077.05	0.10	10.19
JBP	1036.17	1048.17	1078.46	1.51	11.60
LR	1036.91	1048.91	1079.20	2.25	12.34
LC	1035.72	1047.72	1078.01	1.06	11.15
WP	1035.75	1047.75	1078.04	1.08	11.18

TABLE VII: AIC and BIC criteria for the six models dark energy against the Λ CDM for δ_2 (24).

Model	χ^2_{\min}	AIC	BIC	Δ AIC	Δ BIC
Λ CDM	1038.41	1046.41	1066.60	-	-
CPL	1035.36	1047.36	1077.65	0.95	11.05
BA	1034.55	1046.55	1076.84	0.14	10.24
JBP	1035.96	1047.96	1078.24	1.54	11.64
LR	1036.69	1048.69	1078.97	2.28	12.37
LC	1035.50	1047.50	1077.79	1.09	11.19
WP	1035.52	1047.52	1077.81	1.11	11.20

TABLE VIII: AIC and BIC criteria for the six models dark energy against the Λ CDM for δ_3 (25).

Model	δ	χ^2	AIC	BIC	ΔAIC	ΔBIC
ΛCDM	GR	0.29	4.29	8.11	-	-
	δ_1	0.29	8.29	15.94	3.99	7.82
	δ_2	0.29	8.29	15.94	3.99	7.82
	δ_3	0.28	8.28	15.93	3.98	7.81
CPL	GR	0.29	8.29	15.94	-	-
	δ_1	0.29	12.29	23.76	3.99	7.82
	δ_2	0.28	12.28	23.75	3.99	7.81
	δ_3	0.28	12.28	23.76	3.99	7.81
BA	GR	0.29	8.29	15.94	-	-
	δ_1	0.27	12.27	23.75	3.98	7.81
	δ_2	0.28	12.28	23.75	3.99	7.81
	δ_3	0.24	12.24	23.71	3.94	7.77
JBP	GR	0.29	8.29	15.94	-	-
	δ_1	0.29	12.29	23.76	3.99	7.82
	δ_2	0.29	12.28	23.75	3.99	7.81
	δ_3	0.24	12.24	23.71	3.95	7.77
LR	GR	0.29	8.29	15.94	-	-
	δ_1	0.28	12.28	23.75	3.99	7.81
	δ_2	0.28	12.28	23.75	3.99	7.81
	δ_3	0.28	12.28	23.76	3.99	7.81
LC	GR	0.29	8.29	15.94	-	-
	δ_1	0.28	12.28	23.75	3.98	7.81
	δ_2	0.28	12.28	23.75	3.98	7.81
	δ_3	0.27	12.27	23.74	3.98	7.807
WP	GR	0.29	8.29	15.94	-	-
	δ_1	0.29	12.29	23.76	3.99	7.82
	δ_2	0.28	12.28	23.75	3.98	7.81
	δ_3	0.24	12.24	23.71	3.94	7.77

TABLE IX: AIC and BIC criteria for the three delta functions δ_1 (23), δ_2 (24), δ_3 (25) and the six dark energy models and the ΛCDM against the GR model where $D_L(z) = D_S(z)$.